

**PL-TR-96-2252**

**ATMOSPHERIC EFFECTS ON OPTICAL PROPAGATION**

**Patrick McNicholl**

PhotoMetrics, Inc.  
4 Arrow Drive  
Woburn, MA 01801-2067

04 October 1996

Final Report  
01 May 1991 - 29 February 1996

19970623 284

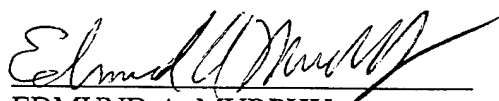
Approved for public release; distribution unlimited

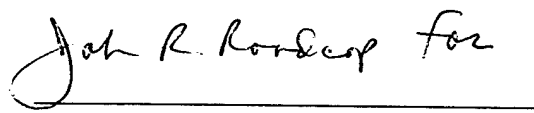
**DTIC QUALITY INSPECTED 4**




**PHILLIPS LABORATORY**  
**Directorate of Geophysics**  
**AIR FORCE MATERIEL COMMAND**  
**HANSCOM AIR FORCE BASE, MA 01731-3010**

"This technical report has been reviewed and is approved for publication"

  
EDMUND A. MURPHY  
Contract Manager

  
ROBERT R. BELAND  
Branch Chief

  
WILLIAM A. M. BLUMBERG  
Division Director

This report has been reviewed by the ESC Public Affairs Office (PA) and is releasable to the National Technical Information Service (NTIS).

Qualified requesters may obtain additional copies from the Defense Technical Information Center (DTIC). All others should apply to the National Technical Information Service (NTIS).

If your address has changed, if you wish to be removed from the mailing list, or if the addressee is not longer employed by your organization, please notify PL/IM, 29 Randolph Road, Hanscom AFB, MA 01731-3010. This will assist us in maintaining a current mailing list.

Do not return copies of this report unless contractual obligations or notices on a specific document require that it be returned.

REPORT DOCUMENTATION PAGE			Form Approved OMB No. 0704-0188	
Public reporting burden for this collection of information is estimated to average 1 hour per response, including the time for reviewing instructions, searching existing data sources, gathering and maintaining the data needed, and completing and reviewing the collection of information. Send comments regarding this burden estimate or any other aspect of this collection of information, including suggestions for reducing this burden, to Washington Headquarters Services, Directorate for Information Operations and Reports, 1215 Jefferson Davis Highway, Suite 1204, Arlington, VA 22202-4302, and to the Office of Management and Budget, Paperwork Reduction Project (0704-0188), Washington, DC 20503.				
1. AGENCY USE ONLY (Leave blank)	2. REPORT DATE 4 October 1996	3. REPORT TYPE AND DATES COVERED Final 91/05/01 to 96/02/29		
4. TITLE AND SUBTITLE Atmospheric Effects on Optical Propagation		5. FUNDING NUMBERS Contract F19628-91-C-0013 PE 62101F PR 7670 TA 15 WU BA		
6. AUTHOR(S) Patrick McNicholl				
7. PERFORMING ORGANIZATION NAME(S) AND ADDRESS(ES) PhotoMetrics, Inc. 4 Arrow Drive Woburn, MA 01801-2067		8. PERFORMING ORGANIZATION REPORT NUMBER PhM-TR-91-0013F		
9. SPONSORING / MONITORING AGENCY NAME(S) AND ADDRESS(ES) Phillips Laboratory 29 Randolph Road Hanscom AFB, MA 01731-3010 Contract Manager: Edmund A. Murphy/GPOL		10. SPONSORING / MONITORING AGENCY REPORT NUMBER PL-TR-96-2252		
11. SUPPLEMENTARY NOTES				
12a. DISTRIBUTION / AVAILABILITY STATEMENT Approved for public release; distribution unlimited			12b. DISTRIBUTION CODE	
13. ABSTRACT (Maximum 200 words)  A program to perform coordinated research employing complementary electro-optical techniques to characterize optical and physical properties of the atmosphere are described in this report. Emphasis was on upgrading and operating the CO <sub>2</sub> wind sensing lidar, upgrading and operating the Nd:YAG backscatter lidar, on working with the multichannel transmissometer, and on upgrading the MAPM system.				
14. SUBJECT TERMS lidar Doppler wind wind sensing DIAL MAPM			15. NUMBER OF PAGES 58	
			16. PRICE CODE	
17. SECURITY CLASSIFICATION OF REPORT UNCLASSIFIED	18. SECURITY CLASSIFICATION OF THIS PAGE UNCLASSIFIED	19. SECURITY CLASSIFICATION OF ABSTRACT UNCLASSIFIED	20. LIMITATION OF ABSTRACT SAR	

## TABLE OF CONTENTS

	PAGE
1. PROGRAM OBJECTIVES	1
2. TECHNICAL PROGRESS	2
2.1 FIRST QUARTER	2
2.1.1 CO <sub>2</sub> LIDAR SYSTEM	2
2.1.2 Nd:YAG LIDAR SYSTEMS	4
2.1.2.1 ANALYSIS OF ABLE RECEIVER OPTICS	4
2.1.2.2 PHOTOMULTIPLIER TUBE FOR SIMULTANEOUS ANALOG AND PHOTON COUNTING OPERATION	5
2.1.2.3 SIMULTANEOUS POLARIZATION MEASUREMENTS	6
2.1.3 MULTICHANNEL TRANSMISSOMETER	7
2.2 SECOND QUARTER	8
2.2.1 CO <sub>2</sub> LIDAR SYSTEM	8
2.2.2 Nd:YAG LIDAR SYSTEMS	10
2.2.3 MULTICHANNEL TRANSMISSOMETER	14
2.3 THIRD QUARTER	14
2.3.1 CO <sub>2</sub> LIDAR SYSTEM	14
2.3.2 RAMAN LIDAR SYSTEM	17
2.3.3 Nd:YAG LIDAR SYSTEMS	17
2.3.4 MULTICHANNEL TRANSMISSOMETER	20
2.4 FOURTH QUARTER	21
2.4.1 CO <sub>2</sub> LIDAR SYSTEM	21
2.4.2 RAMAN LIDAR SYSTEM	22
2.4.3 Nd:YAG LIDAR SYSTEMS	22
2.4.4 MULTICHANNEL TRANSMISSOMETER	25

## TABLE OF CONTENTS (continued)

	PAGE
2.5 FIFTH QUARTER	26
2.5.1 CO <sub>2</sub> LIDAR SYSTEM	26
2.5.2 RAMAN LIDAR SYSTEM	29
2.5.3 Nd:YAG LIDAR SYSTEMS	29
2.6 SIXTH QUARTER	32
2.6.1 CO <sub>2</sub> LIDAR SYSTEM	32
2.6.2 RAMAN LIDAR SYSTEM	33
2.6.3 Nd:YAG LIDAR SYSTEMS	33
2.7 SEVENTH QUARTER	34
2.7.1 CO <sub>2</sub> LIDAR SYSTEM	34
2.7.2 Nd:YAG LIDAR SYSTEM	36
2.8 EIGHTH QUARTER	36
2.8.1 CO <sub>2</sub> LIDAR SYSTEM	36
2.8.2 MAPM	38
2.8.3 Nd:YAG LIDAR SYSTEM	38
2.9 NINTH QUARTER	40
2.9.1 CO <sub>2</sub> LIDAR SYSTEM	40
2.9.2 MAPM	41
2.10 TENTH QUARTER	42
2.10.1 CO <sub>2</sub> LIDAR SYSTEM	42
2.10.2 MAPM	43
2.11 ELEVENTH QUARTER	44
2.11.1 BALLISTIC WIND PROGRAM	44
2.11.2 CO <sub>2</sub> DOPPLER LIDAR SYSTEM	44

## TABLE OF CONTENTS (continued)

	PAGE
2.12 TWELVE QUARTER	44
2.12.1 BALLISTIC WIND PROGRAM	44
2.13 THIRTEENTH QUARTER	45
2.13.1 BALLISTIC WIND PROGRAM	45
2.13.2 CO <sub>2</sub> DOPPLER LIDAR	45
2.13.3 MAPM	46
2.14 FOURTEENTH QUARTER	46
2.14.1 BALLISTIC WIND PROGRAM	46
2.14.2 CO <sub>2</sub> DOPPLER LIDAR/FLD MODE LOCKING	46
2.14.3 MAPM	46
2.15 FIFTEENTH QUARTER	47
2.15.1 BALLISTIC WIND PROGRAM	47
2.15.2 CO <sub>2</sub> DOPPLER LIDAR/FLD MODE LOCKING	47
2.15.3 MAPM	47
2.16 SIXTEENTH QUARTER	48
2.16.1 BALLISTIC WIND PROGRAM	48
2.16.2 CO <sub>2</sub> DOPPLER LIDAR/FLD SPECKLE MEASUREMENTS	48
2.17 SEVENTEENTH QUARTER	48
2.17.1 BALLISTIC WIND PROGRAM	48
2.17.2 CO <sub>2</sub> DOPPLER LIDAR/FLD SPECKLE MEASUREMENTS	49
2.17.3 MAPM	49
2.18 EIGHTEENTH QUARTER	49
2.18.1 BALLISTIC WIND PROGRAM	49
2.18.2 MAPM	50
2.18.3 SBIRS CIRRUS DATA	50

## TABLE OF CONTENTS (continued)

	PAGE
2.19 NINETEENTH QUARTER	51
2.19.1 MAPM	51
2.19.2 BALLISTIC WIND PROGRAM	51
2.19.3 SBIRS CIRRUS DATA	51
2.20 TWENTIETH QUARTER	51
2.20.1 MAPM	51
2.20.2 BALLISTIC WIND PROGRAM	52

## **1. PROGRAM OBJECTIVES**

The objective of this four year program was to perform a coordinated research effort employing complementary electro-optical techniques to characterize optical and infrared propagation through the atmosphere. This effort included measurements of the parameters that affect propagation, at several wavelengths, under meteorological conditions of interest to the DoD.

Under this program PhotoMetrics was to perform acquisition, analysis and interpretation of data using lidar techniques (both coherent and incoherent) and visible and infrared transmissometry. This included:

- Research on the characterization of atmospheric optical extinction and backscatter coefficients by polarization-sensitive and simultaneous multi-wavelength lidar measurements.
- Measuring and modeling the temporal and spatial structure of aerosol scattering density in the troposphere, including cloud layers, by simultaneous remote probing with two Nd:YAG elastic backscatter lidars (0.53 and 1.06 microns) and a ground based multi-spectral visible/infrared transmissometer.
- Designing, implementing, and evaluating a calibration scheme for the lidar systems for the purpose of inferring absolute backscatter coefficient from lidar data and for inter-system correlation.
- Performing research leading to a Doppler wind measurement capability for the GPOL 10.6 micron mobile coherent lidar.
- Conducting measurement operations to map wind fields with the GPOL Doppler lidar facilities and investigating the ability of these systems to detect and characterize localized wind field disturbances of natural (e.g., topographic) and artificial (e.g., aircraft induced) origin.
- Investigation of alternate detection techniques to increase capability and improve performance of GPOL coherent lidar systems. This includes research on the use of balanced heterodyne detection, detector arrays, and newly developed optical fibers.



## **2. TECHNICAL PROGRESS**

### **2.1 FIRST QUARTER**

#### **2.1.1 CO<sub>2</sub> LIDAR SYSTEM**

##### Demodulator

Our initial inspection of the complex demodulator (built by NOAA/WPL) revealed that one channel (the "I" or in-phase) was defective. This was traced to the low pass filter on this channel. To retain the amplitude and phase match of the channels, we replaced these filters on both channels with an available pair of utility 10 MHz low pass filters. This was a temporary measure as the amplitude and phase response of these utility filters is not as flat as the originals. We continued to look into the options for a more permanent fix, e.g., repair/replacement of the faulty filter.

##### Acquisition Software

In the Doppler measurement test phase, we planned to use available CAMAC based DSP 2112F transient recorders for digitizing the demodulated data. These have a 20 MHz maximum sampling rate and allow for recording of Doppler shifts up to 10 MHz corresponding to a velocity of 50 m/s (about 100 mi/hr). During this quarter, we wrote test software to control three synchronized 2112F's (see below) from a PC. This program downloads the results of each laser shot from the CAMAC and then stores the digitized wave forms on a hard disk, ram disk, or in extended memory. In handling heterodyne lidar signals one has two options: (1) "pre-process" the results of each shot to obtain the desired phase independent information and then "signal average" this quantity over a number of shots to improve the SNR; or (2) record the results of each shot and later post-process the accumulated data. The former more easily allows for real or near real time display; however, it requires dedicated pre-processing hardware to attain even a 10 Hz repetition rate. We have adopted for this test phase the latter approach. Its advantages are: (1) no required dedicated analog or digital processing hardware; (2) flexibility in specifying the processing after the data has been obtained; and (3) the data storage rate is the sole limitation to the operational repetition rate. Its disadvantages are: (1) one must cease acquisition in order to process the data and (2) it is memory intensive. To illustrate the second point, we consider the situation where data is to be accumulated covering a 15 km range. This requires transient recorder record lengths of 2048 (at 20 MHz sampling rates). With 2 bytes required per record and two channels (I and Q), the memory required to store the results of a single laser shot is 8 kilobytes. For 10 seconds of data running at 10 Hz, 0.8 Megabytes are required. We have performed preliminary tests of

this single shot acquisition/storage technique using a 386/20 Mhz PC and found that system rep rates up to about 10 Hz are possible if using a hard disk as the memory medium and up to about 20-25 Hz if employing a ram disk in extended memory.

### Processing Software

We have, in addition, written test software to read, display, and process the demodulated data acquired in the manner discussed above. It includes standard techniques for extracting the amplitude and frequency information from the demodulated data as well as utility procedures for absolutely calibrating the frequency response of the amplitude and phase of both the I and Q channels of the acquisition electronics. This processing and acquisition software was written for system test purposes with significant extensions and changes to be made in the future.

### Laser Pulse Characterization

We used the system discussed above to investigate the spectral composition of the TEA laser pulse. It was necessary to characterize the pulse spectral width, frequency chirp, and pulse to pulse frequency jitter in order to compensate for these effects as well as to evaluate the expected Doppler performance. For the measurements, a pick-off from the AFC detector signal was attenuated and delivered to the complex demodulator (operating under low gain). Preliminary results indicate a pulse spectral width of about 1 MHz (FWHM) resulting primarily from chirp. (The Fourier transform width expected for a pulse with the same amplitude and no chirp is about 0.25 MHz.) The frequency jitter varies with laser operating conditions from about 0.5 to 1.0 MHz ( $1\sigma$ ).

### Frequency Monitor

To compensate the Doppler signals for the laser frequency jitter, a frequency measurement for each pulse is necessary. The digital pulse frequency counter (PFC) employed by the laser AFC system has a resolution of only 0.6 MHz so that errors of 1.5 m/s (about 3 mi/hr) would result if we employed the PFC measurement to correct the Doppler data. To overcome this, we tested an available RHG 40 MHz limiter/discriminator. The third transient recorder channel mentioned above was used to record the discriminator output during the laser pulse testing. Good agreement was found between the temporal profile of the pulse frequency obtained from the recorded I/Q data and that recorded directly from the discriminator. A comparison of the peak spectral component of the FFT of the signal to the discriminator voltage at a given time (about 1  $\mu$ sec from the beginning of the pulse) showed a

random discrepancy resulting solely from the resolution of the FFT--about 60kHz. Using the frequency discriminator as a laser frequency monitor allows us to correct for jitter with a resolution corresponding to about 0.3 m/s (0.6 mi/hr).

### Data 6000

Preliminary software was written to allow for recording of the I/Q signals with the Analogic Data 6000. This serves not only as a back up to the CAMAC based system but also to enable tests of the effects of increased digitizing sampling rate. (The Data 6000 is capable of 50 MHz sampling rate in dual channel mode.)

Full up tests of the Doppler system were expected with the return and installation of the telescope. In addition to these tests, the following additions to the system were planned to be worked on in the next quarter:

- improved dust protection for the Brewster windows and grating as well as the receiver deck components;
- a pulse energy monitoring system (pyroelectric detector, S/H circuitry, and A/D conversion);
- frequency monitoring system (aforementioned discriminator, S/H circuitry, and A/D conversion);
- use of a room temperature HgCdTe detector for the AFC system;
- scanner computer interface hardware and software.

## **2.1.2 Nd:YAG LIDAR SYSTEMS**

### **2.1.2.1 ANALYSIS OF ABLE RECEIVER OPTICS**

The receiver optics of the ABLE (Atmospheric Balloonborne Lidar Experiment) lidar system were analyzed to check their suitability for multiple scattering measurements in which the receiver optical axis is deviated from the laser optical axis. (When the outgoing laser beam is not in the receiver field-of-view then the only scattered laser light that is detected is multiple scattered light.) For these so-called off axis measurements to be valid the receiver must have suitable angular resolution and must not allow the passage of light which is out of its field-of-view. Therefore, a ray tracing analysis was performed in order to measure the effects of aberrations on the angle of arrival of rays.

The ABLE receiver is a Dall-Kirkham Casagrain. The primary mirror is f/1, 20 inches in diameter, and elliptical in shape. The secondary mirror is spherical. The distance between the primary and secondary is 16 inches. The back focal length is 24 inches and the

effective focal length is 120 inches. Using these parameters we deduced the curvature of both mirrors from formulas for general two reflector systems in "The Infrared Handbook" (p. 9-20). The curvature of the primary is  $-0.025 \text{ inches}^{-1}$ . The curvature of the secondary is  $-0.104 \text{ inches}^{-1}$ .

The ray tracing code was used to determine the parameter which describes the ellipticity of the primary lens. This was done by having the program search for the value of that parameter which minimizes the spherical aberration of the telescope (i.e., the size of the blur at the focal plane when rays parallel to the optical axis are input). The result is a "shape factor" ( $1 - \text{ellipticity}^2$ ) of 0.2199. This is to be compared to a theoretical calculation using formulas for the 4th order aspheric deformation (The Infrared Handbook, p. 9-22) of 0.2269.

After determining the layout of the optics the ray tracing code was used to study the angular resolution of the telescope. A series of sets of parallel rays across the telescope aperture were input, for a number of different angles with respect to the optical axis. The percentage of rays to pass through to the focal plane, and the rms blur size of the resulting spot were determined. We found that the rms blur size varies from 0.001 inches for rays parallel to the axis to 0.003 inches for rays at angles of 0.002 radians. (The full angle field-of-view of the receiver is specified as 0.004 radians.) A transverse spatial separation of 0.001 inches in the focal plane corresponds to an angular separation of 10 microradians in object space. Therefore, the telescope angular resolution is very good.

Almost 100% of the rays which enter the receiver with angles less than 0.00185 radians make it to the focal plane. 80% of the rays with angles of 0.0019 radians make it to the focal plane. No rays with angles greater than 0.002 radians get to the focal. Therefore, there is no danger that single scattered rays will be detected when the receiver field-of-view does not include the outgoing laser beam.

We concluded that off axis measurements to study multiple scattering are feasible with the ABLE receiver.

#### **2.1.2.2 PHOTOMULTIPLIER TUBE FOR SIMULTANEOUS ANALOG AND PHOTON COUNTING OPERATION**

A signal channel for simultaneous photon counting and analog detection of 532 nm radiation for the TOADS (Transportable Optical Atmospheric Detection System) lidar was tested in the laboratory and was determined to be ready for operation. The detector was a gated photomultiplier tube (Thorn EMI 9954B with the G1004B gating circuit). The PMT output went to a LeCroy VV100B pulse amplifier, a 150 MHz amplifier which is capable of driving two 50 ohm loads. One load was a transient recorder for analog detection. The other

load was a LeCroy MV104PK comparator and a DSP 2190 multichannel scalar for photon counting. These components were purchased, tested, and were almost completely operational on a previous contract. The only part which needed additional work was the gated photomultiplier tube.

Previously, a Hamamatsu R263 photomultiplier tube had been purchased. However, it was found that this PMT could not be gated properly with the EMI G1004B gating circuit. The tube response was not constant for constant light input during the gate. A linear focus type tube with a separate gating grid is necessary. Thorn EMI recommended the 9954B.

We tested and verified the operation of the 9954B for gating operation and for simultaneous photon counting and analog operation. We had to rewire the gating circuit for the new tube and change a few components in the dynode chain for proper operation. We tested the tube in the laboratory using an LED as a source. The output of the tube was linear up to approximately 1 mA of anode current. (The tube was tested for gate widths of 100 microseconds and gate spacings of 25 msec and a variety of cathode to anode voltages up to 2200 V). The average anode current was approximately 4 microamps. The maximum recommended anode current was 200 microamps on average. The dynode chain current for 1800 V between the cathode and anode was approximately 1 mA. The usual rule of thumb is that the dynode chain current should be at least 10 times the anode current. Therefore, the tube was quite robust.

### **2.1.2.3 SIMULTANEOUS POLARIZATION MEASUREMENTS**

We designed and were building a modification to the TOADS receiver which allows for simultaneous measurement of two crossed linear polarizations of the backscattered 532 nm radiation. The 1064 nm channel was to be removed and replaced with an additional 532 nm channel. The current photomultiplier tube was to be used for one channel and the Thorn EMI 9954B photomultiplier tube described in the previous section was to be used for the other channel. This channel would also be capable of simultaneous photon counting and analog operation. (Therefore, this channel would be used for measuring polarization parallel to that of the laser beam.)

The new second channel was to be constructed inside a box which could be attached to the back of the existing receiver. Minimal modification to the existing receiver was needed so that there will be no interruption to lidar operation during construction. It would be possible to put the 1064 nm channel back in if desired.

A polarizing beam splitter (Melles-Griot 03-PBS-037) was to be used to split the backscattered 532 nm radiation into two linearly polarized beams. One beam, which had polarization parallel to that of the laser, was reflected by the beam splitter by 90 degrees and sent along the existing optical path (i.e., through the existing filter and lens which images the primary onto the photocathode of the PMT). The other beam, polarized perpendicular to that of the laser beam, was transmitted through the beam splitter. It was then reflected through 90 degrees by a mirror and then sent through a lens to be imaged to the photocathode. The lens was a symmetric convex f/1 with a focal length of 2 inches (Melles-Griot 01-LDX-115). The photocathode was placed at the focal point of the lens (instead of at the location of the image of the primary) because the blur diameter is approximately 5 cm. This should be compared with the 1 cm diameter photocathode. (Calculations performed with a ray tracing code). Given the distances involved a simple lens could not be specified which would image the primary to the photocathode with an image plus blur size less than 10 cm.

The TOADS laser (Litton model ILS-NT-254) was sent to Litton (Apopka, Florida) for refurbishment. This included repolishing the doubling crystal, realigning and replacing cavity optics, and overall optimizing performance. Prior to being sent to Litton the laser output energy was about 1/10 of its optimum at 1064 nm. (Typical energy at 1064 nm is 120 mJ/pulse.)

When Litton returned the laser, we tested it and found that its energy was 120 mJ/pulse for pulse rates less than or equal to 10 Hz. At 20 Hz the energy was 90 mJ/pulse. We typically operated at 20 Hz and preferred to have 120 mJ/pulse.

### 2.1.3 MULTICHANNEL TRANSMISSOMETER

Calculations were done which lay the groundwork for modeling the performance of transmissometers operating in rain. A program was written to generate total and differential Mie scattering cross sections for raindrops in the 0.25 to 5mm radius range. Attempts to model the 0.53  $\mu\text{m}$  transmissions measured by the Phillips Laboratory Multichannel transmissometer during FLAPIR had limited success. Raindrop distributions (size and spatial) in the transmissometer path were inferred from Rain Distrometer data. The program calculated the direct and scattered (single scattering) components for the selected rain distribution and transmissometer geometry. Results for very high rain rates appeared to correspond well to actual measured transmission values. As the droplet concentration decreased the model program predicted transmissions much higher than measured. It was assumed that this was due to the fact that fog was also present at this time (aerosol particle size

distributions were not available because this equipment could not be operated in the rain). The assumed transmissometer geometry needed further refinement and the raindrop velocity vs. size necessary to determine droplet spatial concentrations needed to be verified. Addition of "fog" to the model may be necessary for comparison with the FLAPIR data.

## **2.2 SECOND QUARTER**

### **2.2.1 CO<sub>2</sub> LIDAR SYSTEM**

#### Frequency Correction

During the second quarter of the program we tested two different methods of correcting for the laser frequency jitter: (a) recording the demodulated temporal laser pulse profile along with the demodulated backscatter signal (see below); and (b) using a frequency discriminator on the AFC laser signal. Our analysis of the data indicated that both methods were capable of yielding corrections to better than 1 m/s. The first method provides complete information on the pulse characteristics and is not subject to analog component drift; however, the second method is much faster for either real time or post-acquisition processing.

#### Sample and Hold Circuit

We completed a two channel sample and hold circuit for the monitoring of both the laser pulse energy and frequency. The first (slow) channel has a 30 kHz full power bandwidth sufficient for sampling the output of an integrating pyroelectric energy detector and holding this value for sampling by an A/D channel to be added to the data acquisition system. The second channel is faster (200 V/microsec slew rate) in order to sample the output of the frequency discriminator at a representative time during the laser pulse. An alternative output was built for this second channel with gain and offset control sufficient to allow direct substitution of this signal for that from the PFC (Pulse Frequency Counter) unit employed by the laser AFC system. This provides a backup for the PFC unit. In comparison to the PFC, the sampled discriminator output has much greater resolution (on the order of 0.06 MHz compared to 0.6 MHz) but will be more subject to long term drifts. We started developing an A/D card driver in the acquisition software to enable recording of these signals. In addition, construction of a pyroelectric detector was initiated for dedicated use by the pulse energy monitor.

#### RF Switch

A fast GaAs switch was incorporated into the complex demodulator after the amplification stages but before the mixers. This allows for injection of the AFC signal into the demodulation/acquisition stream for the first 5 to 10  $\mu$ sec. Due to initial backscatter from the shared T/R optics, the signal during this time is not of interest and the inclusion of the laser pulse with each recorded shot allows for inspection of the pulse temporal profile as well as correction for frequency jitter.

#### Reverse Bias/PreAmp

Test data runs revealed small but significant artifactual baseline features in the signal averaged data. These effects were found to result from the large initial signal pulse due to the initial scatter from the shared T/R optics. We made additional tests which indicated that the origin of these baseline effects was a transient response of the HgCdTe diode junction characteristics or bias level, or of the preamplifier. We redesigned the preamplifier and bias circuit to decrease the recovery time of the diode junction bias voltage. This was done to decrease the dead time after the laser fires and to decrease the (much later) transient effects.

#### System Noise Levels and LO Power

Preliminary data reduction indicated a system noise level several times greater than that expected from nominal detector/amplifier performance. Since, in a heterodyne detection scheme, the noise power depends upon LO power we constructed a test box to facilitate direct measurement of the LO power incident upon the detector. For planned future system noise and sensitivity tests this would allow for systematic evaluation of nominal vs. actual system performance.

#### Scanner Drive

We assisted with development of the scanner drive software.

#### Data Processing Software

We greatly expanded a data analysis program to include FFT's and frequency correction techniques for the determination of wind velocity as well digital IIR filters for extraction of backscatter power from the demodulated signal.

In addition, we attended a meeting with representatives of Canetics Inc. on the Doppler acquisition and processing system that they are currently developing for OPA. We also transmitted to Canetics information on the detector, amplifier, and demodulation electronics as well as the characteristics of typical test data.



### 2.2.2 Nd:YAG LIDAR SYSTEMS

#### Laser

The Nd:YAG laser used for the low altitude lidar system (Litton model ILS/NT-254) was returned from Litton Laser, Inc., CLS Division in South Windsor, CT. The laser had been sent there in the last quarter because its energy output at 20 Hz pulse repetition rate was low. (The energy output at 10 Hz was normal.) This was the result of an incomplete refurbishment, in the last quarter, by Litton Laser in Apopka, FL. The laser was brought up to specifications at 20 Hz (120 mJ/pulse at 1064 nm and 25 mJ/pulse at 532 nm). After the laser was returned the lidar system was reassembled and made operational.

#### Photon Counting System Performance

The performance of the new photon counting system was evaluated. Backscattered 532 nm radiation from volcanic dust, clouds, and aerosols, was acquired and analyzed. Polarization measurements of this backscattered radiation were made.

Photon counting and current mode acquisition of the backscattered 532 nm radiation were performed simultaneously, with the same photomultiplier tube. The photomultiplier tube (Thorn EMI 9954B) output signal is fed to a LeCroy VV100B 200 MHz pulse amplifier. This amplifier is capable of driving two 50 ohm loads. The amplifier output is split along two pathways. The signal along one pathway is integrated and sent to a transient recorder for current mode acquisition. The other pathway is sent to a discriminator and multichannel scalar averager for photon counting. Each path is 50 ohms as seen from the output of the pulse amplifier. The discriminator incorporates a LeCroy MVL104 400 MHz voltage comparator. The multichannel scalar averager (DSP model 2190) is capable of counting at rates up to 100 MHz. Thus, the maximum rate at which the photon counting system can count photons is limited by the scaler.

We evaluated the performance of the photon counting system with backscattered radiation from the atmosphere. Photon counting of the backscattered 532 nm radiation during clear nights revealed the existence of a layer of volcanic dust (Mt. Pinatubo) with a peak density at 22 km and a thickness (full width at half maximum) of approximately 3 km. We also observed less dense, but broader, layers at 15 to 16 km and at 18-19 km. We describe this data below in more detail. Here we describe the signal for the purposes of illustrating the performance of the photon counting system.

The maximum count rate we observed was approximately 40 MHz. If the system is set up such that for a given range the count rate is 40 MHz then the count rate for nearer ranges is

observed to be less than 40 MHz (even though the true rate of arrival of photons is higher). For farther ranges the count rate decreases because of the decrease of the true rate of arrival of photons. We calculate that the rate at which the photon counting signal is valid is approximately 0.71 times the maximum measured count rate (28.5 MHz). This assumes the number of photons per unit time is described by a Poisson probability function and that two or more photons arriving in a time interval equal to the width of a photon pulse is counted as one photon.

Based on these calculations the maximum theoretical count rate (for a scaler capable of counting as high) is 70 to 140 MHz. This is based on the observed width of a photoelectron pulse at the output of the discriminator to be in the range of 5 to 10 nsec. The maximum valid count rate would therefore be 50 to 100 MHz. Additional testing of the photon counting system needed to be performed to increase the maximum observed count rate of 40 Mhz.

For data acquired at the Phillips Laboratory parking lot on the (clear) night of Sept. 28, 1991, with 1800 Volts between the anode and cathode, 20 mV discriminator level, 25 mJ/pulse of laser energy at 532 nm, and lidar elevation of 90 degrees, the peak count rate of 40 MHz is observed for an altitude of 1.9 km. The signal is valid at approximately 2.1 km. (The validity of the signal is evident by looking at the R squared corrected signal, which decreases approximately exponentially.) The signal was sky background limited. The background count rate of sky background photons was approximately  $15000 \text{ sec}^{-1}$ , about 20 times the dark count rate for 1800 Volts. The sky background was about 10 times the "theoretical" rate (Handbook of Geophysics) probably because of the lights in the parking lot and elsewhere at Hanscom AFB.

#### Photon Counting System Data

The photon counting system extended the maximum range at which the lidar operates. By photon counting we observed volcanic dust at 22 km and Rayleigh and aerosol scattering at altitudes below the dust. Furthermore, the degree of polarization can be calculated for all these data with much greater accuracy than for the analog channel data. With the analog channel the lidar could not detect the volcanic dust layers and it could only detect aerosol scattering up to altitudes of approximately 5 km. If the scattering ratio of these aerosols was near one (i.e., near Rayleigh scattering) then the lidar could only detect aerosol scattering up to approximately 2.5 km.

Several nights of backscatter data from the volcanic dust layers were acquired using the photon counting system. The analog channel could not detect the dust layers. The data revealed that the layer centered at 22 km was very stable at least during the period of a few

weeks. The lower layers, however, change (both density and thickness). The optical thickness of the 22 km layer was in the range of 0.034 to 0.053 (depending on the model used to analyze the data) (analysis done by LTC G.G. Koenig). The optical thickness for all the layers on one particular night (Sept. 28, 1991) is in the range of 0.044 to 0.068. Thus, most of the optical depth was due to the 22 km layer.

Using the polarizers inside the lidar receiver revealed that the backscattered radiation from the dust retains the polarization of the laser radiation. Therefore, the dust particles were close to spherical. The optical depths were too low to expect much multiple scattering.

The backscattered radiation from altitudes below the volcanic dust indicated that Rayleigh scattering was predominant for altitudes above approximately 10 km. Below approximately 5 km aerosol scattering dominated. Polarization studies showed that the backscattered radiation from these altitudes had degree of polarization of 0.97 (a degree of polarization of unity indicates complete polarization). Since we did not expect to observe depolarization from Rayleigh backscattering we concluded that the laser radiation had a degree of polarization of 0.97.

Some backscatter data from high thin cirrus clouds was collected. The cirrus cloud data was acquired by accident, when a cirrus cloud happened to be drifting through the lidar volume while acquiring data for some other purpose. The cirrus clouds which had been observed did not have a measurable effect on the backscattered signal from the volcanic dust, thus indicating a very small optical depth.

Polarization measurements of the backscattered radiation from a cirrus cloud were made on Oct 24, 1991. The data were acquired as the cloud drifted by at an altitude of 9.3 km (with a thickness of approximately 450 m, or three data bins). The degree of polarization, with the Rayleigh/Mie baseline subtracted out of the parallel component, was 0.16. Because of the low optical depth of the cloud this relatively low value could only be due to asphericity of the particles and not multiple scattering.

#### Current Mode Channel

Data from the current mode channel revealed a nonuniform response of the photomultiplier tube during the early part of the gate on period. In response to a constant light level source the output signal of the photomultiplier tube rose to approximately 0.9 of its steady state value in the first 2 microseconds after the tube was gated on. This 2 microsecond rise time was an expected characteristic of the tube operating with the gating circuit. It was factored out of the signal through a calibration procedure. The problem was that the signal

continued to rise to its full steady state value in the next 10 microseconds after the initial fast rise.

This problem had been reported in the past, as well as attempts to correct it. Some success had been achieved by modifying the dynode chain circuit which was shipped with the tube from the manufacturer (Thorn EMI). However, the problem had never completely gone away.

In the last quarter, engineers at EMI suggested an alternative tube which might not suffer from this problem when used with the gating circuit. The alternative tube (9817) was identical to the tube we used (9954) except it had an S20 photocathode instead of a bialkali photocathode. S20 has a smaller resistivity than the bialkali. Thorn EMI loaned us a 9817 tube to evaluate. We received the tube and found that it suffered from the same problem. We returned the 9817 to Thorn EMI.

We decided to use the present tube and correct for the slow rise time by the same calibration procedure that we used to correct for the earlier fast rise time. Our tests showed that the tube's response during the slow rise time was linear (as was the case during the fast rise time as well). An extension to the look up table used to correct for the fast rise time (correction factors as a function of time and anode to cathode voltage) was made.

The slow rise time did not affect the photon counting data. The amplitude of each photoelectron pulse is affected by this problem, not the number of photoelectrons which occur.

### Simultaneous Polarization Measurements

Construction of a housing, and related parts, for a second 532 nm data channel for simultaneous crossed polarization measurements was completed. The new channel replaced the existing 1064 nm channel. The housing was to be mounted on to the back of the lidar receiver and would extend approximately 4 inches outside the lidar enclosure. A hole would be drilled in the lidar enclosure wall to accommodate the housing. The avalanche photodiode/amplifier box currently located at the back of the lidar receiver would be removed. The housing was designed to make a light tight seal against the lidar receiver.

The housing included optics to relay one linear polarization component of the 532 nm radiation to a second photomultiplier tube. The two crossed polarizations (perpendicular and parallel to the polarization of the outgoing laser radiation) were separated with a polarizing beam splitter. The polarizing beam splitter replaced the dichroic beam splitter currently used to separate the 1064 nm and 532 nm radiation.

### 2.2.3 MULTICHANNEL TRANSMISSOMETER

Changes were made to the PL/OP Mie scattering codes MIE2B and MIE3B to allow them to be executed on an IBM compatible PC under Fortran 4.1. The changes were primarily to the BLOCKDATA initialization routines and placing some variables into named common blocks. The card image input structure was retained. Both programs can duplicate the results of test cases in the "User's Guide for the Mie Scattering Codes at AFPL."

Problems were encountered trying to use MIE3B to calculate the attenuation due to large water droplets--relative uncertainties in extinction and scattering were approximately 50% (non-convergence messages were issued by the program). It is likely that this can be corrected by performing the calculations in double precision (comparable to the 60 bit precision of the CYBER) for which the programs were originally written. The large double precision complex arrays will not fit into the PC data space allowed with this version of Fortran and considerable rewrite of the programs would be necessary.

Encouraging results were obtained with a very simple algorithm to simulate the operation of the PL/OP Multichannel Transmissometer during periods of rain. Raindrop size distributions obtained using a Particle Measurement Systems Rain Distrometer and empirical droplet fall velocities were used to determine the droplets in the scattering volume. Total and forward scattering of droplets as a function of radius were obtained from another program which performs a full Mie solution for real index of refraction particles. The transmissometer algorithm determines transmission as the percent of the acceptance angle of the optical system which is blocked by particles of a given Mie cross section placed at random distances along the path. The enhancement of transmission due to the high forward scatter from raindrops is treated as an "unblocking" of a fraction of each Mie cross section. Calculated and measured transmissions at 0.53 micrometers during a 17 minute period agreed to within 5%.

## 2.3 THIRD QUARTER

### 2.3.1 CO<sub>2</sub> LIDAR SYSTEM

#### Scanner

During the third quarter we assisted with development of the software to run the scanner. This package runs on a 80286 computer and can receive commands from the keyboard or over a serial line. We incorporated scanner control functions into the lidar data acquisition and control program using this asynchronous communication channel.

## CAM IQ

The preliminary operating system was single shot based, i.e., the demodulated I and Q signals resulting from a single laser shot were digitized by a synchronized pair of DSP2112 transient recorders and transferred using DMA to the host computer (presently a 20 MHz 80386). Under what we refer to as standard conditions: 20 MHz sampling rate and record lengths of 2048 (sufficient for 15 km range coverage), slightly less than 40 msec was required to transfer the 8kBytes of data. Thus, 25 Hz was the maximum operating repetition rate. Cam\_IQ configures up to 64 shot buffers for this data in lower memory so that a number of shots can be acquired at the maximum rate without pausing for storage or analysis. We added an extended memory buffer system which increased the number of shots held in memory to about 700. This data can be manually stored to disk or the system can be requested to automatically write to disk when the buffers are full.

An assembler module was developed for data display. Due to its direct addressing of VGA memory this module is capable of plotting the data in real time under standard conditions and at slightly greater than 10 Hz repetition rates. By reducing the requested plot coverage greater repetition rates can be achieved. Buffered data (either just acquired or read back from disk) can also be "replayed" at up to about twice the real time acquisition rate.

An FFT module was written to handle the specialized data shot record buffers. The inner loop of this FFT algorithm was written in assembler to decrease the execution time. This module actually performs two transforms in selectable range windows of the data. Typically, the first window is on the section of the signal into which the AFC laser signal has been inserted and hence provides the laser frequency. This FFT module can be activated in two different ways. The first mode, single shot, performs the double FFT on a per shot basis and displays power spectra for the laser window and the range window. Due to the plotting procedure, this mode has a maximum repetition rate of about 6 Hz but is very useful for evaluating system performance and inspecting local wind conditions prior to data taking. The second mode uses the results of the laser window transform to correct the data window transform for frequency jitter and accumulates the range window power spectrum for a selectable number of shots. Only at the end of this accumulation is the result displayed so that operation at 10 Hz should be possible.

## Canetics

We sent information to Canetics, Inc. on the laser and IF electronics specifications as well as plots of sample data sets to aid them in system design. We also evaluated a processor board, the VCE1, which they delivered to GPOA. This analysis indicated that this board,

which employs a single DSP32C floating point processor, is capable of speeding up the FFT's by a factor of at least 10 over that obtainable with the present host. A full evaluation was not possible due to the limited software package included with the board. They agreed to deliver a more complete package.

There were several reasons for this evaluation: (1) becoming familiar with the programming of the DSP32C which would be required for the final Canetics system; (2) evaluating the suitability of reduction algorithms (e.g., FFT) to the architecture of the DSP32C; and (3) possible inclusion of the VCE1 in the IQ\_CAM operating system. The latter could provide sufficient transform speed for real time acquisition in up to 20 range windows at a 10 Hz repetition rate.

### Electronics

A number of minor electronic modifications and tests were made. We buffered the input trigger to the GaAs range gating circuit to eliminate the previous unreliable performance at some delay/width selections. An intermittent problem with one of the Allen Avionic low pass filters in the complex demodulator was traced to a bad internal BNC connection. This filter was returned for repair. Evaluation of the S/H circuitry for laser energy and frequency showed a non reproducible droop sufficient to affect performance. We designed a digital hold circuit which will eliminate this problem. We evaluated the performance of the log amplifier and 70 MHz limiter/discriminator provided under the GE contract. The components checked out to specs and the log amplifier provided a useful display of backscatter signal. The use of the discriminator for Doppler measurements, as proposed by GE, was --as expected--found to be restricted to ranges where the signal-to-noise was large. In practice, only about 1 km vertical coverage could be expected.

### Baseline Artifacts

Significant signal baseline features were found to result from the large initial signal pulse due to backscatter from the shared transmit/receive optics. During this period, we made a number of tests which identified the primary source of this backscatter as the secondary mirror surface and cover plate. The scatter from the latter was reduced greatly by constructing a new cover plate with better surface characteristics and by aperturing upstream from the secondary. The surface scatter itself remains as the dominant source, although inclusion of a couple of apertures in the receiver optics has reduced this by about a factor of four. The amount of this scatter reaching the detector was found to be extremely sensitive to alignment.

This reduction in the scatter decreased but did not eliminate the baseline effects. If, as these tests indicated, scatter from the secondary mirror surface was the dominant source of the initial light pulse, no optical methods, other than the aperturing which we had already inserted, can further reduce this problem without a complete system redesign. During the next period, we determined whether the detector or preamplifier is the ultimate source of the baseline response to the scatter pulse.

### GABLE Analysis

We assisted with calibration and reduction of ground based lidar data taken on the GABLE measurement program.

In addition, we assisted with constructing covers for the transmit receive optics and remounting of the scanner camera monitor.

## **2.3.2 RAMAN LIDAR SYSTEM**

During this period, we worked with B. Dix on the optical layout of the receiver for the mobile Raman lidar system and assisted with the trailer layout of the various system components. In addition, we met with GPOA concerning the data acquisition software for this system.

## **2.3.3 Nd:YAG LIDAR SYSTEMS**

### Simultaneous Polarization Measurements

Work continued on modifying the lidar receiver to simultaneously detect radiation polarized parallel and perpendicular to the laser. A housing, and related parts, for a second 532 nm data channel was fabricated. The second data channel replaced the existing 1064 nm data channel. The dichroic beam splitter which separated the 532 nm and 1064 nm radiation was replaced with a polarizing beam splitter.

A filter holder was made to hold a two-inch diameter 532 nm filter for the new channel. The filter holder is attached at the location of the existing 1064 nm filter and lens. A mount for the polarizing beam splitter was fabricated. The mount fits into the same location occupied by the existing mount holding the dichroic beam splitter.

Modifications of previously fabricated housing parts were made in order to attach the photomultiplier tube and related optics. Careful placement of various holes for these attachments needed to be done so that the radiation is directed properly to the photomultiplier



tube photocathode. There is capability to make some fine adjustments to the optics once they are in place and nominally aligned.

The lidar receiver/detector box was removed from the lidar system in order to check the fit of the newly fabricated parts. A new back plate for the lidar detector box needed to be fabricated in order to attach the new housing. All newly fabricated parts were anodized and were ready for permanent placement into the detector box.

#### New Trailer-Mounted, Nd:YAG Lidar System

A general qualitative design for a new Nd:YAG lidar system was devised. The lidar will employ a roof-based scanning system which will relay the laser radiation and backscattered radiation from/to the inside of the trailer. The lidar will employ two receivers. One receiver will use a twelve inch Dall-Kirkham telescope previously designed and partially built for the TOADS lidar system. The other receiver will employ a twenty inch Dall-Kirkham telescope previously used for the ABLE lidar system.

The twelve inch telescope will be used as the "primary" receiver. Its field of view will contain the outgoing laser radiation and will sense both single scattered and multiple scattered radiation. The twenty inch telescope will be used as the "secondary" receiver. Its field of view will not contain the outgoing laser radiation and will therefore only sense multiple scattered radiation. It will be steerable using the existing scanning system previously employed by the ABLE lidar.

The primary receiver will be equipped to measure elastic scattered 355 nm, 532 nm, and 1064 nm radiation from the doubled and tripled Nd:YAG laser. In addition, it will be capable of making simultaneous crossed polarization measurements of the 532 nm radiation. Furthermore, it will be equipped with two channels to measure Raman scattered radiation from water and nitrogen. All these channels will not necessarily operate simultaneously due to constraints of the data acquisition system. Photomultiplier tubes will be used to detect all radiation except the 1064 nm elastic backscattered radiation which will use a silicon avalanche photodiode.

We have done signal/noise calculations for the proposed lidar system for both the elastic scatter and Raman scatter channels. Below we present a few representative values of signal/noise ratio (S/N) per laser shot. S/N increases as the square root of the number of laser shots. We consider three noise processes: 1) shot noise in the signal, 2) sky background, and 3) detector noise.

Elastic backscatter channel (assuming Rayleigh scattering and a 1976 U.S. Standard atmosphere):

<u>Wavelength (nm)</u>	<u>Altitude (km)</u>	<u>S/N (day)</u>	<u>S/N (night)</u>
355	1	1000	1000
532	1	600	600
1064	1	350	350
355	10	4.5	30
532	10	2	20
1064	10	1	1
355	30	0.02	2.5
532	30	0.01	2
1064	30	0.0035	0.0035

For near ranges S/N is shot noise limited for all wavelengths. For far ranges during the day S/N is sky background limited for 355 nm and 532 nm, but detector noise limited for 1064 nm. For far ranges during night S/N is shot noise limited for 532 nm, but detector noise limited for 1064 nm. Note that S/N for the 1064 nm channel does not vary from day to night, indicating the detector noise limitation.

For the Raman channels we have considered Raman scattered radiation from nitrogen and water vapor for both 355 nm and 532 nm incident radiation. It turns out that both wavelengths produce about the same S/N for each species. For nitrogen the two possible Raman transitions are 355-->387 nm and 532-->607 nm. For water vapor the two possible Raman transitions are 355-->408 nm and 532-->660 nm. We will choose (for practical considerations in the design of the detector) nitrogen Raman at 607 nm and water vapor Raman at 407 nm.

The S/N calculations for the water Raman channel considers a mid-latitude mean water vapor model from the 1976 U.S. Standard Atmosphere. Raman S/N calculations are only done for night (daytime S/N is too low to be viable with proposed filters). The only noise process considered is shot noise in the signal.

<u>Wavelength (nm)</u>	<u>Altitude (km)</u>	<u>S/N</u>
607 (N <sub>2</sub> )	1	20
407 (H <sub>2</sub> O)	1	2
607 (N <sub>2</sub> )	4	3.5
407 (H <sub>2</sub> O)	4	0.25
607 (N <sub>2</sub> )	8	1.5
407 (H <sub>2</sub> O)	8	0.035
607 (N <sub>2</sub> )	12	0.75
407 (H <sub>2</sub> O)	12	0.004

#### 2.3.4 MULTICHANNEL TRANSMISSOMETER

Work continued on calculating or modeling transmission through rain using data obtained during the FLAPIR program (July 1990, Brunswick ME). The decision was made to utilize an existing and accepted Mie scattering code (PL/OP Mie scattering code MIE2B) rather than construct and justify a new code. The modeling has been based upon the measured raindrop size distributions obtained from a Particle Measurement Systems Rain Distrometer which was operated during FLAPIR. MIE2B is used to calculate volume extinction and scattering coefficients and the angular scattering phase function from the particle size distributions which were obtained at one minute intervals (average over one minute).

A major question which could be settled by these calculations is the apparent discrepancy in extinction values measured during periods of heavy rain by two different PL/OP instruments (the Multichannel Transmissometer and an HSS Visibility Meter). While for light rain, extinctions from the two instruments agreed during heavy rain the visibility meter or forward scatter meter consistently measured extinctions two to five times higher than the transmissometer. Explanations may be : 1) the forward scattermeter overestimates extinction in rain; 2) high forward scatter from large raindrops increases the amount of light reaching the transmissometer detector (underestimation) ; 3) a combination of the above.

While the size distribution from the PMS distrometer may be converted to number densities using a model for droplet velocity versus size, this can be avoided initially by simply calculating the rain rate (in mm/hour) from the size distribution and using the Marshall-Palmer rain model for number densities needed by the scattering code. This simplification of the distribution function appears not to affect the scattermeter which depends only on the volume extinction coefficient but may somewhat alter the response calculated for the transmissometer.

It should be noted that there are some questions about the precision of the measurements by the distrometer, namely undercounting due to overload in heavy rain, counting overlapping small drops as a larger drop, undercounting due to end element rejection, and overcounting due to splashing during heavy rain. Measurements concurrent with the operation of a calibrated rain gauge would probably resolve these questions.

Scattering calculations for the visibility meter using all of the PMS data showed that the relationship  $r = 10 (v - 0.01)$  where  $r$  is extinction and  $v$  is the measured instrument voltage is valid (that is,  $r$  calculated from the scattering (27 - 42 degree) matches the extinction coefficient from MIE2B and also compares well with the measured  $r$ . Implementing the Mill-Shettle snow model technique for the transmissometer and using the same droplet distribution did not yield good agreement between measured and calculated  $r$ .

## **2.4 FOURTH QUARTER**

### **2.4.1 CO<sub>2</sub> LIDAR SYSTEM**

#### Scanner

During this period, we continued development of the software/hardware to run the scanner. With the inclusion of a software selectable locking option this package was essentially complete. Scanner control from the lidar data acquisition and control program using asynchronous communication was tested. At present, the system operator can select scan speeds, enable or disable lock, have the scanner execute basic "go-to" operations, or select a data acquisition mode which steps through azimuth angles as velocity data is being collected. Possible future additions to this software package were considered: parallel operation of the data acquisition and scanner control computers; continuous scan modes; and raster ("imaging") scan modes.

#### CAM-IQ

We significantly increased the baseline repetition rate of the data acquisition system by employing a block mode for DMA was of data from the CAMAC to computer RAM. Single shot data transfer time decreased from about 40 to 14 msec enabling I/O limited repetition rates up to 70 Hz.

System tests revealed a problem with synchronization of the modules used for digitizing the I and Q channels. Although both modules were operated with the same external clock, independent triggering resulted in occasional offsets of one bin time (50 nsec) in their relative start time. This presumably resulted from internal logic operating on an asynchronous

clock. We now operate the external clock in a triggerable burst mode with the A/D modules' software triggered well in advance of the clock trigger.

Preliminary gain/phase calibration procedures were included in CAM\_IQ to digitally correct for imbalances in the demodulator channels. Use of these procedures revealed a glitch in the DMA procedures used to download the data from the CAMAC. The code used to break up a block DMA transfer if it crosses a 64kB page boundary (supplied by DSP, Inc.), apparently loses a data point resulting in an IQ relative phase shift thereafter. We avoided the difficulty by manipulating memory assignment so that page boundaries always line up with data sets. (A maximum of 4kB of RAM is wasted in this fix-up.)

Full-up tests of this single data window system were performed with real time velocity-azimuth plots generated for ranges out to 8 km. Signal-to-noise conditions indicated that increased ranges are obtainable depending on atmospheric conditions.

### DSP32C

We received from Canetics, Inc. software necessary for communicating with and programming of their DSP32C based VCE1 card. Software units for use of this card for signal processing by CAM\_IQ were nearly completed. Preliminary performance estimates were that up to 40 Hz system Doppler operation with complete range processing could be possible depending on the complexity of the algorithms involved. Obtaining the highest possible rates is dependent on parallel operation of the VCE1 card and the CAMAC data download. Tests of a CAM\_IQ version incorporating the VCE1 card were to be completed soon. This would be the last major system change in the Doppler system prior to delivery, installation, and evaluation of the system being constructed by Canetics.

### **2.4.2 RAMAN LIDAR SYSTEM**

During this quarter, we worked on the optical layout of the receiver for the mobile Raman lidar system and assisted with the trailer layout planning of the various system components. In addition, we had meetings concerning the data acquisition software for this system.

### **2.4.3 Nd:YAG LIDAR SYSTEMS**

#### Second 0.53 micron channel

The lidar system was equipped with a second 0.53 micron channel. The purpose of the second channel was to make simultaneous crossed polarization measurements of the

backscattered 0.53 micron radiation from the atmosphere. The final parts comprising the channel were completed and anodized early in the quarter. The lidar receiver was removed from the lidar enclosure in order to install the second channel and test it in the laboratory. The back plate of the lidar enclosure was also removed. It was modified in order to allow the new channel to fit into the system. After testing, simultaneous polarization data from the atmosphere (specifically, clouds and volcanic dust) were acquired and analyzed.

The second channel replaced the 1.06 micron channel. A box was fabricated to fit onto the back of the lidar receiver where the 1.06 micron detector and amplifier were located. The box contained the appropriate optics for directing radiation to a second photomultiplier tube. Additional parts were fabricated for holding a polarizing beam splitter which separates the 0.53 micron radiation along two paths. The path with the backscattered radiation polarized parallel to the laser was directed along the previously existing path. The other polarization was directed along the new path. The polarizing beam splitter replaced a dichroic beam splitter previously used to separate the 0.53 micron and 1.06 micron backscattered radiation.

The previously existing optical path (parallel polarization) used the newer photomultiplier (Thorn EMI 9954B) tube and was set up to operate simultaneously in analog and photon counting mode. The new channel (perpendicular polarization) used the older photomultiplier tube (EMI Gencom G21D711BG). It was set up to operate both in analog mode and photon counting mode, but not simultaneously. We used a Pacific Instrument AD6 amplifier/discriminator with this tube for photon counting. We used a second DSP Technology 2190 multichannel scalar averager to count and average the photocounts as a function of range.

Bench tests in the laboratory with unpolarized light and hand held polarizers indicated the two channels to be operating correctly. The polarizing beam splitter was approximately 98% efficient. That is, approximately 2% of the wrong polarization was passed along both pathways.

### Simultaneous Polarization Measurements

Backscatter data was acquired using the modified lidar receiver. Simultaneous crossed polarization measurements from clouds, volcanic dust, and snow were acquired and analyzed. The cloud and snow data were acquired with the photomultiplier tubes operating in analog mode. The volcanic dust data were acquired with the photomultiplier tubes operating in photon counting mode.

We calculated depolarization ratios from the data of the two channels. The two channels had different transmissivities and the photomultiplier tubes had different gains and

responses. During daytime operation the two channels were calibrated relative to each other by equating sky backgrounds and baselines of both channels. The sky background, which was assumed unpolarized, was acquired between laser pulses. The baseline was data acquired before the system trigger.

During nighttime, if both tubes were operating in photon counting mode, then there was enough sky background detected (at least in the Phillips Laboratory parking lot) to calibrate both channels with respect to each other in the same manner as described above. When operating in analog mode we calibrated the channels with respect to each other by using previously calibrated response curves for both photomultiplier tubes (as a function of anode to cathode voltage) along with previously measured transmissivities for both optical paths. This was somewhat less accurate than equating sky background.

The cloud data that we acquired included low strato-cumulus at 1.5 to 3 km as well as cirrus clouds at 8 to 10 km. We found the lower clouds to have depolarization ratios that approached 0.5 after a few hundred meters into the clouds. We found cirrus cloud depolarization ratios on the order of 0.1. Using the strato-cumulus cloud data we also saw a correlation between the depolarization ratio and the delay between the peaks of perpendicularly polarized and parallel polarized backscattered radiation (i.e., a higher depolarization ratio had a smaller delay, which was consistent with the idea of multiple scattering).

The volcanic dust, which was spread over a wide altitude region from 13 km to 23 km, showed depolarization ratios of approximately 0.05 to 0.1. This was contrasted with the volcanic dust data acquired in Sept/Oct of 1991, which showed no depolarization. That data also showed the dust to be concentrated in two layers: a lower density one at 15 to 16 km and a higher density one at 20 to 23 km.

The cloud data was compared with a double (Mie) scattering program which had been developed by PhotoMetrics for a related contract with GPOA. The code took as input the extinction coefficient as a function of range and the particle size distribution (assumed constant with range). The outputs of the code were the perpendicular and parallel components of the doubled scattered radiation within the field-of-view of the receiver, and the single scattered radiation.

We used the double scattering program to deduce particle size distributions in clouds. We derived extinction coefficients as a function of range from the lidar data using single scatter assumptions (e.g., the Klett inversion technique) and used this as input to the double scattering program. We assumed different size distributions until we made a good match between data and model. The figure of merit that we used to test for a match was the

depolarization ratio. We typically assumed "modified gamma" size distributions with the mode radius and spread as free parameters.

#### Measurements in Sudbury, MA

The lidar was moved to Sudbury, MA to participate in a cloud measurement program along with diagnostics sensitive to other wavelengths (e.g., a 35 GHz incoherent backscatter radar and a Platinum Silicide (3-5 micron) video camera). For these measurements we set the lidar up to make simultaneous crossed polarization measurements at 0.53 microns. The 1.06 micron channel was not present. We took some preliminary backscatter data on clouds. Simultaneously acquired data existed for the 35 GHz radar. The radar sensed two cloud layers centered at 1.5 km and 5 km. The lidar sensed only the lower layer for most of the data set. Occasionally, a hole in the lower layer allowed for detection of the upper layer.

#### **2.4.4 MULTICHANNEL TRANSMISSOMETER**

Work continued comparing modeled and measured extinctions through rain and fog during the FLAPIR program (July 1990, Brunswick ME). Directly measured extinctions were available from two different GPOA instruments - the Multichannel Transmissometer and an HSS Visibility Meter.

Model data for rain periods was calculated using the GPOA Mie scattering code MIE2B utilizing the Marshall-Palmer rain distribution. The rain rate needed for the Marshall-Palmer was reduced from measured raindrop size distributions as a function of time obtained from the Particle Measurement Systems Rain Distrometer which was operated during FLAPIR. Droplet size range was 0.1 to 6.2 mm. Model extinction for fog periods was reduced from three aerosol size distrometers which were operated during clear and fog conditions measuring particle size distributions for sizes 0.15 to 133  $\mu\text{m}$ . NRL calculated the extinction at several wavelengths from these data. Our calculations of extinction from MIE2B using these size distribution data matched the extinctions provided by NRL.

An implementation of the Mill-Shettle snow model for single scattering was used to calculate model extinctions for the transmissometer using extinction and scattering coefficients derived from size distributions by MIE2B. Since similar scattering calculations for the visibility meter showed that  $\tau$  calculated for its 27-42 degree acceptance angle matched the extinction coefficient from MIE2B the latter extinction was used as the model for the visibility meter. Angular scattering calculations for different size water droplets showed that the visibility meter measurement should be nearly totally insensitive to particle size while the



transmissometer measurement is highly dependent on size due to the increasingly highly peaked forward scatter as droplet size increases.

Comparisons of measured and modeled extinctions did not resolve the differences observed between transmissometer and visibility meter measurements and probably indicated that aerosol and rain droplet size distributions alone contained insufficient information to model the extinction as measured by particular instruments. While spatial variation and the difference between point and path measurements may account for some of the observed deviation, there is an inconsistency of comparison more likely explained by incompleteness or error in measurement of the size distributions. The precision of measurement by the rain distrometer may be influenced by undercounting due to overload in heavy rain, counting overlapping small drops as a larger drop, undercounting due to end element rejection, and overcounting due to splashing during heavy rain. The aerosol distrometers may be subject to some of the same problems (they are of generally similar construction) -counting overload, overlap and end element rejection - and mechanical aspiration is known to influence the measurement of particulate distributions.

## **2.5 FIFTH QUARTER**

### **2.5.1 CO<sub>2</sub> LIDAR SYSTEM**

#### **IQV1**

This Doppler lidar operating system is a descendent of CAM\_IQ which used assembler routines to perform the core data processing functions (e.g., FFT's, digital filters,...). IQV1, though modularly similar, transfers the single shot data to the VCE1 board RAM (using DMA) which processes the data and either transfers the results (e.g., velocity vs. range) back to the host memory or accumulates these results for a set number of shots. Single shot data transfer times from the CAMAC to the host RAM (about 14 msec) limit maximum system repetition rates to 70 Hz. The system is capable of operating at this speed but only to accumulate the data in host RAM buffers with no processing. About 6 msec are required to transfer the single shot data record from host to VCE1 RAM so that real time processing is presently I/O limited to 50 Hz  $[=1/(14 \text{ msec} + 6 \text{ msec})]$ . The CAMAC to host transfer of a shot record is done in parallel with the DSP32C processing of the previous record. Under these conditions 35-40 Hz full range Doppler operation was achieved with the processing including shot-by-shot corrections for laser frequency jitter as well as baseline fluctuations. About 45 Hz operation is possible employing a digital filter to obtain received backscatter power versus range.

Although there is some room for speed improvement of the processing algorithms, the data transfer times are the major limitation on speed. A significant speed improvement could be obtained by parallel host to DSP32C memory transfer and processing. The DSP32C DMA handler is capable of this and Canetics, in their Phase I report, stated that they tested this operation on the VCE1 board. However, our tests were unsuccessful in that a significant number of errors appeared in data transferred to the DSP32C memory during the processing of the previous pulse.

This operating system for the CO<sub>2</sub> lidar is preliminary in that at some future date it will be replaced by the dedicated A/D and processor boards currently being built by Canetics. However, for near term operation (envisioning possible delays in the satisfactory installation of the new system) and as a future possible hardware/software data acquisition system for MAPM, we felt that improving the performance and reliability of IQV1 was important. In this light, we followed up on the aforementioned and other methods to increase the present I/O limited repetition rate. In addition, we felt that consideration should be given to obtaining a second DSP32C card as backup since the existing card was a single point failure for the data acquisition system. The code could also be easily changed to employ a second DSP32C if available. This would ensure attainment of the present I/O limited repetition rate (50 Hz) while allowing for almost twice the present single shot processing time.

A number of other features were included in IQV1: processing for backscattered power as well as velocity; capability for variable record length download from the CAMAC; advanced triggering of the acquisition to enable realtime measurement and compensation for noise power levels; and utilities for laser and detection performance measurements.

### Performance

Extensive operational performance tests were made for system sensitivity as well as Doppler operation. A summary of these was presented at the 16<sup>th</sup> International Laser Radar Conference held in Cambridge in July 1992. Briefly, system calibration measurements indicated that (1) operation allowed for a sensitivity about 3 dB below the shot noise limited regime and (2) the system sensitivity was an additional 3 dB below that obtained from *ab initio* calculations. Operation at higher LO power levels and modifications of the detector bias circuitry would allow for near shot noise limited operation. The measured versus expected sensitivity discrepancy could arise from a number of sources: (1) incorrect characterization of the atmospheric extinction on the days calibration measurements were done and/or of the transmission/reflection of the optical system components; or (2) a deviation from the assumed wavefront properties of the LO and TEA beams. As we were somewhat conservative in our

estimation of former, we suspected that wavefront deviations were the source of most of the discrepancy.

The LO beam was known to be astigmatic due to the curved grating used in the cw laser oscillator. Although we corrected for its expected astigmatism in the calculations, we did not have the capability to confirm the assumed wavefront shape or the degree of collimation of the LO at the beam expander. Moreover, since the LO beam size after the stock beam expander was oversized for a match to the TEA beam an iris was employed. Without intensive diffraction calculations precise compensation for the effects of this iris on sensitivity were difficult to make. The expected and actual system sensitivity could be improved (and possibly made to agree) by eliminating the LO astigmatism and building/purchasing a custom beam expander. The former can be achieved by replacing the grating in the MPB cw CO<sub>2</sub> laser with a curved mirror. If operation on only strong CO<sub>2</sub> lines (e.g., P20) is envisioned this poses no operational problems. A custom beam expander with fine adjust capability can be obtained for a moderate price, although modification of an existing beam expander could be done for a somewhat lower price.

During far field (about 12 km) hard target system tests, the turning mirrors in the scanner were found to have a small curvature so as to act like a slight converging element in the optical transmit/receive system. This effect agrees in magnitude with that expected from surface figure measurements made by Tucson Optical. We compensated for this to first order by adjusting the telescope focal distance; however, since these mirrors were used at 45 degrees incidence, they would introduce astigmatism in the far field even if their surface figure were ideally spherical. In addition, the Mersenne telescope design is not ideal for use at other than infinite conjugate ratio.

Tests identified two main sources of noise pickup in the analog data acquisition circuitry: (1) common mode AC pickup, and (2) ground noise resulting from the PFC box. Floating the signal return line at the input to the 1020 differential amplifier eliminated the former whereas grounding it eliminated the latter. To eliminate both without rewiring the PFC, we capacitively coupled the return line to ground at the 1020 effectively low pass filtering the return line so that the low frequency common mode AC pickup remained unaffected. Although this worked, the appropriate fix would be to modify the PFC. Inspection of this unit and its circuit diagrams revealed that the digital return was not properly isolated from the analog common and chassis ground with the result that digital ground spikes were coupled straight into the chassis and rack ground, contaminating all the grounds of electronics in this rack. Extensive remounting of the two PFC boards would be required to fix this.

In addition, we have found two paths by which the IF signal was contaminated with AOM sourced 40 MHz pickup. The first was RFI pickup at the detector to preamp lead and was eliminated with shielding. The second path was optical: backscatter from the AOM of 40 MHz shifted light was transported through the cw laser optics into the LO beam. To reduce this we planned to move attenuation devices from their present position between the AOM and the TEA laser to before the AOM. In addition, we planned to ascertain whether careful alignment of the AOM could reduce this backscatter.

### **2.5.2 RAMAN LIDAR SYSTEM**

During this quarter, we worked on the optical layout of the receiver for the mobile Raman lidar system and assisted with the trailer layout of the various system components. In addition, we had discussions concerning the data acquisition software for this system. We worked on installing the excimer laser in the trailer and bringing it up to specifications. We also began evaluation of a R878 PMT gating circuit for possible use in the backscatter channel.

### **2.5.3 Nd:YAG LIDAR SYSTEMS**

#### Simultaneous Crossed Polarization Measurements from Water Clouds

We made simultaneous crossed polarization measurements of water clouds with the lidar and compared the data to a double Mie scattering computer program developed for a related contract with PL/GPOA. Our goal was to validate the model and use it to determine size distributions and multiple scatter corrected extinction coefficients of water clouds.

Our technique was to determine the range resolved extinction coefficient from the lidar data using the Klett technique, and run the double scatter model with this extinction and many different size distributions. For simplicity, we chose a particular functional form for the size distribution (e.g., modified gamma) with one or two free parameters that can be varied (e.g., mode radius and distribution width). We then chose the best size distribution by comparing the measured (range resolved) depolarization to the calculated depolarization from the model. Using the return power predicted by the model we then recalculated the extinction coefficient (this was then the multiple scatter corrected extinction) and reran the model to better estimate the size distribution.

In our initial work in comparing the model results to the data we found, in some cases, depolarization ratios for water clouds which were larger than what could be predicted by the model. During the rest of this quarter we pursued issues and possible problems with the

measurements which we felt would serve to either verify or invalidate this discrepancy. We discuss these below.

**1) Variable response of telescope with respect to angle of incidence.** One reason the calculated depolarizations could have been low is because the model considers a lidar telescope with a constant response with respect to angle of incidence of the incident rays. This was not the case for the actual lidar telescope. We know from previous work (using a ray tracing code) that the angular response of the primary lens coupled with the field stop was not constant. It was higher for zero degrees incidence and fell off monotonically for greater angles. To determine the angular response of the entire optical system we completed the ray tracing analysis by including the rest of the optical components. We found that the response was approximately flat (with a transmittance of 0.01) from angles of incidence of zero to approximately 10 mrad. It then increased to a peak (0.035) at 15 mrad and then decreased monotonically. The transmittance was essentially zero at 25 mrad. We included this angular response in the double scatter computer model. The predicted depolarizations were then higher for such a response compared to a constant response since the off non zero incidence rays, which are more depolarized, are weighted more heavily. However, the depolarizations were not high enough to agree with the measured depolarizations.

**2) Use of a different interference filter for both channels.** The primary reason for discrepancy between lidar measurements and model was that each channel of the lidar receiver (the parallel and perpendicular polarization components) used a different interference filter. The "parallel" channel used an older one inch diameter filter that was used before the receiver was modified to perform simultaneous crossed polarization measurements. The "perpendicular" channel used a two inch diameter filter originally planned for a new lidar receiver. Different filters in each channel, by themselves, were not a problem. The problem arose because we calibrated the two channels with respect to each other by using the unpolarized background light. This led to a discrepancy if the two filters had different values of the ratio of transmissivity of white light to transmissivity of doubled Nd:YAG light. There was no reason to expect that this ratio was the same for two different filters. Especially, two filters manufactured three years apart and with different specifications, as was the case for the two filters being used. Therefore, to alleviate this problem we identified a location inside the receiver where a single filter could be used by both channels. The location could only accommodate a one inch filter. We removed the receiver from the lidar system, we removed the two inch filter, and we moved the one inch filter to this common spot. We reinstalled the lidar receiver and attempted to take lidar data.

Unfortunately, after having done this, the lidar receiver would not respond to doubled Nd:YAG backscattered radiation. We thought that the reason for this was the poor state of the older one inch filter that was being used for both channels. It had degraded significantly through the years. We ordered a new one inch filter from Barr Associates in Westford, MA. While awaiting the new filter we removed the one inch filter from the system and acquired data during nighttime. The receiver did detect doubled Nd:YAG radiation without the filter at night.

**3) Saturation of photomultiplier tube used for parallel polarization channel.** The data acquired during nighttime had depolarizations high compared to that predicted by the double scatter model. We felt a possible reason for this was that the photomultiplier tube used for the parallel channel was saturated. That is, in these situations, the anode current was too high, putting the tube in a nonlinear regime. We investigated this problem by studying the tubes (for both the parallel and perpendicular channels) on the bench to characterize the parameter regime for which they are saturated (as a function of anode to cathode voltage).

In addition, we built a new amplifier for the parallel PMT (for use during current mode operation) so that higher voltages could be achieved for the same anode currents. The parallel photomultiplier tube output had been fed to a pulse amplifier (LeCroy VV100B) with a 50 ohm input impedance. (This amplifier was used because it could be used to perform current mode and photon counting measurements simultaneously since it can drive two 50 ohm loads.) The photomultiplier tube for the perpendicular polarization channel used an amplifier with a 1200 ohm input impedance. The new amplifier which we built for the parallel PMT was modeled after the one for the perpendicular PMT. Therefore, it too had a 1200 ohm input impedance. Voltages 24 times higher than those attained previously with the LeCroy amplifier could now be attained without the use of additional amplification after the PMT. Therefore, since the nonlinear regime was characterized by a certain anode current, the nonlinear regime now occurs for voltages 24 times higher. We intend to use the LeCroy amplifier for photon counting operation.

We acquired lidar data from a water cloud during nighttime (without an interference filter) and with the input signals to the PMTs within the linear regime which are well characterized. We found agreement between measured depolarizations and calculated depolarizations for certain choices of size distribution.

Two new interference filters were received. We installed one of the filters in the receiver. We took data during the afternoon of a hot day (filter temperature was 35 degrees Celsius). We found that the receiver did not detect doubled Nd:YAG light. It did detect background. We went out at night and took data. The lidar did respond to doubled Nd:YAG

light (with the filter in place). The filter temperature was 25 degrees Celsius. We went out during a cool morning during which the filter temperature was approximately 27 degrees Celsius. We found that the receiver did respond to doubled Nd:YAG light. We took data the next afternoon (filter temperature 33 degrees Celsius). The receiver did not respond to doubled Nd:YAG light. We concluded that the filter was shifted in wavelength too far (to detect Nd:YAG light) when its temperature is above approximately 30 degrees Celsius. Our original design criteria to Barr Associates was that the filter should operate correctly for temperatures between 12 and 30 degrees Celsius.

#### Sixteenth International Laser Radar Conference (ILRC)

Richard Garner attended and presented a talk at the 16th ILRC held on the campus of the Massachusetts Institute of Technology during July 20 to July 24, 1992. The talk was entitled "Determining Water Cloud Particle Sizes from Lidar Depolarization Measurements and Time Dependent Multiple Scattering Calculations." The talk presented results of comparisons between lidar depolarization measurements and calculated depolarizations, as discussed above. A related poster was presented entitled "Time and Polarization Dependent Double Scattering Calculations of Lidar Returns from Water Clouds." The poster discussed the double scattering model in more detail than could be covered in the talk.

## **2.6 SIXTH QUARTER**

### **2.6.1 CO<sub>2</sub> LIDAR SYSTEM**

Our major effort in this quarter was directed towards preparing the Doppler lidar for planned ballistic winds field tests. This included software improvement/additions and testing, some new hardware development and acquisition of spares, and assisting with Doppler lidar wind analysis.

The present Doppler lidar operating system--IQV3--is a descendent of IQV1. During this quarter a number of features were added to the software, including realtime power baseline compensation, velocity-azimuth display (VAD), VAD-fitting to obtain realtime altitude profiles of wind velocity, as well as plotting of these altitude profiles. Spare DSP32c boards were obtained from Canetics, Inc. and tested. Testing and preparation of this software for field tests was ongoing.

### **2.6.2 RAMAN LIDAR SYSTEM**

During this quarter, we worked with on the optical layout of the receiver for the mobile Raman lidar system and assisted with the trailer layout of the various system components. In addition, we had meetings concerning the data acquisition software for this system. We installed the excimer laser on the trailer and brought it up to specifications. The major task was identifying the source of poor performance at other than very low rep rates as a broken magnetic fan clutch inside the laser cavity. We replaced this component with subsequent excellent operation of the laser. We installed cables for control of the scanner drive as well as communication between the data acquisition and the laser control computers.

### **2.6.3 Nd:YAG LIDAR SYSTEMS**

The lidar trailer was relocated from the Sudbury site back to the Phillips Laboratory parking lot. While the lidar system was unavailable for use during the move the laser was taken to PhotoMetrics for testing. Toward the end of the Sudbury campaign we discovered that the laser output energy was lower than normal at both the primary and secondary wavelengths (10 mJ at 532 nm, 90 mJ at 1064 nm).

When we opened the laser we discovered that the Pockels cell had some discoloration, which appeared to be due to burned coating, and two small pock marks (indentations) on one surface. We were able to clean the discoloration with methanol. We were not able to get rid of the pock marks. After doing this the 1064 nm energy was back to normal (120 mJ without the doubling crystal). However, it was taking several minutes to come up to its normal operating level.

Although the 1064 nm energy was back to normal the 532 nm energy was still below normal. We discovered an air bubble inside the doubling crystal mount and the doubling crystal had a cloudy appearance. We sent the doubling crystal to Quantum Technology (Lake Mary, FL), the manufacturer of the crystal, for repair. They repolished the crystal, cleaned it, and replaced the two quartz windows that were responsible for producing the cloudy appearance. The 532 nm energy was then back to normal (26 mJ).

We reinstalled the laser into the lidar system and aligned the system (and proceeded to acquire lidar data (both polarizations) from cumulus clouds.

We performed some tests on the Thorn EMI 9954B photomultiplier tube that was used to measure the 532 nm backscattered radiation which was polarized parallel to the laser. We had seen some unusual behavior during the course of taking lidar data. We discovered that the



tube should not be operated with an anode to cathode voltage less than approximately 1200 volts.

We also tested the Santa Fe Research Corporation MCS-II multichannel scaler averager which had been received early in the summer. The MCS-II is a board which operates inside a PC. It is used for photon counting and it is a lower cost alternative to the DSP 2091 CAMAC based multichannel scaler averager. The MCS-II comes with a menu driven software package for immediate operation.

## **2.7 SEVENTH QUARTER**

### **2.7.1 CO<sub>2</sub> LIDAR SYSTEM**

Our major effort in this quarter was carrying out wind field measurements for the ballistic winds program. This included setup of the lidar at Eglin AFB, repairing shipping damage (see below), operation of the lidar during gunship missions, and later reduction of the data. The details are discussed below.

#### Damage Report

During setup of the lidar in the field, a number of moderate to serious malfunctions of the system were found. Ostensibly, these were due to shipping problems: (a) a rough trip and (b) opening of a roof hatch during shipment. The latter was probably caused by the former and may have resulted in freezing conditions. A brief list of malfunctions follows:

- the radiator internal to the TEA laser discharge chamber was ruptured;
- the water flow solenoid valve in the cooling system would not function;
- the helium gas flow regulator was broken;
- the pulse frequency counter (PFC) in the AFC system developed a short;
- the cw CO<sub>2</sub> laser discharge tube was broken;
- the optics table had come partially loose during shipment with vibrations resulting in a number of optical components becoming loose; notably the telescope primary had rotated within its mounts.

The TEA laser was completely disassembled and the radiator was repaired (silver soldered). The faulty solenoid valve was found and removed from the water flow system. For initial operations, we borrowed a helium regulator from the equipment for the tether sonde

and later purchased a suitable replacement from a welding supply house. The short in the PFC was found and repaired. The spare CO<sub>2</sub> discharge tube shipped with the trailer was installed in place of the broken one. Because of the degree of replacements/adjustments involved in these repairs extensive re-alignments of the lidar were also required.

During the second day of planned operation, the scanner computer malfunctioned (probably unrelated to shipping). Although spare computers were available, the digital I/O card used to read the angle encoders was damaged. No data was lost as a result because the gunship mission was scrubbed due to weather. This occurred on a Friday with the next scheduled mission on Monday. During the weekend, C. Trowbridge of PhotoMetrics shipped to us a compatible card from his micropositioning apparatus. In addition, as a fall-back, we modified the acquisition software to ease as much as possible a manual scanning mode. The card arrived Monday morning and was installed in a spare computer.

### Operation

Wind data was obtained in concert with gunship missions on four days (12/2/92, 12/8/92, 12/10/92, 12/11/92) with smaller test and calibration sets taken on three other days. The operational data sets covered roughly four hours with about 30 complete azimuth scans each. Real-time reduction in the field showed good agreement with wind measurements made by radio- and tether- sondes as well as in situ gunship determinations of wind at altitude. A number of minor software modifications were made in the field for operational convenience and output velocity data formatting.

### Reduction

During January, we performed extensive analysis of the field trip data for wind velocity versus altitude. This included preliminary modifications of the acquisition/processing code to incorporate procedures for handling "bad" data points and weighted VAD fits as well as distortion produced by horizontal wind gradients. In addition, we made a statistical analysis of measurement error and wind deviations from uniform models. The results of this first study were supplied for presentation at a Ballistic Wind results meeting.

### Canetics Acquisition Hardware

During this period, we considered the suitability and required modifications of the new Canetics acquisition hardware. We expect that during the next quarter we will make extensive

tests of the component hardware involved, e.g., the "Aardvark" transient recorder and the "Guppy" i860 card.

### **2.7.2 Nd:YAG LIDAR SYSTEM**

During this period we acquired nighttime lidar data from cirrus clouds at altitudes in the range of 8-9 km. The data were acquired using the photomultiplier tubes in photon counting mode. The polarization of the returns was determined using the two available channels on the lidar system.

In addition the data included returns from volcanic dust. The volcanic dust, presumably from the Mount Pinatubo eruption in the summer of 1991, was spread over a wide altitude range from approximately 10 km to 25 km. The dust did not measurably depolarize the backscattered lidar radiation.

In analyzing cirrus cloud data to determine depolarization we discovered that (variable) background light leaking through the sides of the lidar receiver was leading to erroneous conclusions. This was due to our inability to apply our usual technique of relatively calibrating the two channels using background light entering through the receiver aperture. This had not affected the analysis of polarization data taken with the photomultiplier tubes in current mode because of the lower sensitivity of the receiver in this mode. To alleviate this problem we removed the receiver from the lidar system for laboratory bench testing.

## **2.8 EIGHTH QUARTER**

### **2.8.1 CO<sub>2</sub> LIDAR SYSTEM**

#### System Repetition Rate

Since the maximum repetition rate of the lidar system was limited by the FFT processing of the data to about 30 Hz, we added an additional VCE3 DSP32c processing card and modified the data acquisition code (IQV5) to use one or two such cards. If IQV5 detected two such cards, the destination for data from sequential shots was alternated. Paralleling in this way allowed for processing at greater than 60 Hz. However, the maximum operable rep rate was limited by the CAMAC to host and host to VCE3 data transfer rates. By rewriting the CAMAC to host transfer software we were able to bypass the DSP4101 Signal Averaging Memory and speed up the transfer to enable system operation at 60 Hz. These modifications reduced the time for 16 azimuth, 1000 shots/azimuth scans from about 8 to 5 minutes. No

further significant increases in system speed are possible without replacing the CAMAC based A/D front end, e.g., with the VME/VXi based A/D's or the Canetics dual channel A/D.

Although Canetics had informed us that the VCE3 boards would operate with system clocks up to 64 MHz, two of the three such cards exhibited significant errors when clocks greater than 50 MHz were used. In addition, it was not clear whether the VCE3 board port addresses could be varied sufficiently without PROM/PAL/GAL changes to allow for the simultaneous use of more than two. Since the system speed was essentially I/O limited, use of an additional card would not increase repetition rate but would allow for more elaborate processing.

#### Gated Integrator

A gated integrator feature was added to IQV5 to allow a visual chart like display of signal power, noise power, or radial velocity versus time. This greatly increased the ease of evaluating the effects of system modifications as well as optimizing optical/electronic adjustments.

#### LO/Detector Bias

The bias circuit output load impedance was decreased to better couple detector output to the preamp input and allow for greater LO power levels (up to about 0.7 mW). These modifications improved attainable SNR's by 3 to 6 dB.

#### LO Alignment

The LO beam expander mount was modified to allow for easier adjustments. In addition, we instituted a new LO alignment procedure. In this new procedure, the retro'd HeNe beam used to align the receiver optics is further retroflected to provide a visible spot along the LO path back to the attenuators. Aligning the LO to this HeNe beam provided a much more reliable LO to transmit axis alignment.

#### Miscellaneous

The large baseline jitter of the demodulated signal was significantly reduced by (1) using a single 40 MHz source for the AOM and the demodulator and (2) AC coupling the DSP2112 A/D inputs. Two parallel I/O boards (one as a spare) were purchased for the scanner system to replace the one which malfunctioned during the Eglin tests. Minor rewiring and signal buffering were necessary due to differences between the new and old boards.

### Eglin Data Reduction

We wrote a program to numerically integrate the ballistics trajectory for 40 mm and 105 mm shells fired from nominal gunship orbits and with lidar measured windfields as inputs. Comparison of the code results to the Eglin data indicated a strong correlation of miss vectors with the deviation between the true wind field and an assumed constant "ballistic wind".

### **2.8.2 MAPM**

During this quarter we arranged for the shipping of the MAPM system trailer from Boulder, Co to Hanscom AFB. We began testing and repair of subsystems as well as specifying replacement components. The cw CO2 lasers were cleaned up, tested, and operated nominally. Testing and inspection showed that both TEA laser modulators had missing or failed components and that one of the high voltage power supplies had failed. By interchanging parts, one complete TEA laser power supply was assembled and readied for test. The necessary parts for the other were specified and ordered.

### **2.8.3 Nd:YAG LIDAR SYSTEM**

We performed an extensive bench-top relative calibration between the two polarization channels of the lidar receiver. This was necessary because we were deriving erroneous depolarization values from lidar data from water clouds and clear air. The erroneous values were due to the fact that the lidar receiver was extremely sensitive, when used in photon counting mode, to very small light leaks. A very small difference of leaked light arriving at the two channels could lead to erroneous results.

On the bench we tested the receiver for light leaks. We used the Santa Fe Energy Research Corp. multi-channel scaler averager, model MCS-II. This is a PC based board which could count up to 100 MHz with dwell times as low as 2 microseconds. It is ideal for bench testing but can also be used for data taking. We found that the system had numerous light leaks, which were sealed.

Before relatively calibrating the system we performed a pulse height analysis of the PMTs of both channels to determine the best operating parameters (high voltage and discriminator level) in photon counting mode. We did this by photon counting at specific high voltage levels for different discriminator level settings. We found that we had been operating the perpendicular PMT with a poor choice of high voltage and discriminator level. The parallel tube had been used with satisfactory parameters but we found a better set of

parameters. The following parameters were determined for operating the PMTs in photon counting mode:

	<u>Perpendicular channel</u>	<u>Parallel channel</u>
high voltage:	-1600 V	-1900 V
discriminator level:	-50 mV	-300 mV

These operating parameters were to be used when the perpendicular and parallel PMT were both used with an AD6 amplifier/discriminator.

After eliminating the light leaks and finding the best operating regimes for the PMTs we relatively calibrated the two channels. We did this by using a very stable (in energy) tungsten light source. We placed a series of polarizers in a variety of configurations in front of the source and photon counted with both channels simultaneously, while the background room light was as close to zero as possible. The various polarizer configurations that we used were:

- 1) one parallel polarizer,
- 2) two parallel polarizers,
- 3) one perpendicular polarizer,
- 4) two perpendicular polarizer, and
- 5) one parallel and one perpendicular polarizer.

With this set of configurations, we were able to calculate the relative calibration as well as cross talk between the two channels and transmission of the polarizers to the allowed and crossed polarization. We found cross talk between the channels to be in the neighborhood of 1.5 to 2%. The transmission of the polarizers agreed with the manufacturer's specifications. The parallel polarization channels measures 1.4 times the number of photons that the perpendicular channel measures.

After relatively calibrating the two channels in photon counting mode we checked the validity of our technique of relatively calibrating them in analog mode. Our technique was to use background light, during data taking, as an unpolarized light source that should be measured as equal levels by both channels. However, this technique had problems because of the receiver's varying sensitivity with respect to angle of incidence of the light at its aperture. The background light entered at all allowed angles while the backscattered lidar light entered in a small range of angles (approximately 2 mrad) about the optical axis. It was necessary to divide the perpendicular channel signal by 1.4 after using the background light as a calibration

source. After extensive bench testing the lidar receiver was placed back in the lidar system and the lidar was made operational.

## **2.9 NINTH QUARTER**

### **2.9.1 CO<sub>2</sub> LIDAR SYSTEM**

#### "Real-Time" Ballistics Software

Two programs were written to allow for speedy data analysis in the field. The first--RWND--was written to read, compare, display, and edit wind data from the PL/GPOL and the NOAA Doppler systems as well as standard radiosonde data. The selected/edited wind profile data is written by this program in a commonly formatted output file. Thus formatted, the wind data is read by a second program--MBW (Modifiable Ballistic Winds)--for analysis of the effects of the true wind field on the trajectory of the bomb. Minor alterations were made in these programs in the field--mostly in the values of default parameters and to compensate for NOAA data format changes. The basic result of MBW, as employed in UTTR, was an effective ballistic wind (dependent not only on wind field but also on aircraft release parameters). This value (speed and direction) was communicated to the B52 crew on alternate releases to use in the Gravity Weapon Delivery System in place of the wind at altitude. In preparing for the UTTR trip, ambiguities in the NOAA and radiosonde data formats led us to adopt such an ad hoc approach of adding a second code (RWND) instead of introducing unknown complexities into MBW.

#### CO<sub>2</sub> System Operation

In general, the Doppler lidar performed very well; however, like the previous field trip (Eglin) there were problems associated with the improperly functioning air ride trailer suspension. In particular, several optical mounts had effectively been shaken apart and had to be repaired. In addition, the AOM began leaking coolant water. This problem was thought also to be related to excessive vibrations. On the return trip, the TEA laser bellows flanges broke due to the plasma chamber breaking free of its restraints and the telescope secondary translation mount had bottomed out--despite being locked.

Initial field tests indicated that the PL/GPOL system performed comparably to the NOAA system despite the 7-10 times greater transmitted pulse energies of the latter. Much of the performance advantage of the PL/GPOL system arises from its realtime software processing which allows for spectral power accumulation and signal discrimination.

The extensive running time during the mission allowed us to examine several system problems: notably the DC baseline and azimuth dependent performance issues mentioned in earlier reports. It was very clear after inspection of the data that the azimuth related problem was due to scanner mirror astigmatism: data taken along azimuths where SNR dropouts occurred at 5-10 km showed enhanced SNR at lower ranges (0.5-1 km) indicating a net optical system focus which was dependent on the orientation of the erstwhile flat scanner elevation mirror.

The addition of AC coupling between the demodulator and A/D's and unification of 40 MHz clocks reduced the baseline jitter greatly; however, the system was now apparently limited by small but significant shot-to-shot waveform jitters caused by scattered light from the telescope secondary and possibly rhomb striking the detector. It was felt that some of this problem could be reduced by a 10-20 MHz high pass filter between the detector and preamp or the preamp and demodulator. It was planned to test this idea in the next quarter.

### **2.9.2 MAPM**

Work continued in this quarter on the repair, refurbishment, and redesign of the MAPM DIAL system.

#### CW Lasers and LO Optics

Envisioning at least initial use of the UltraLaserTech cw CO<sub>2</sub> lasers, the locking and offset systems were checked and found to be operational. In addition, the LO chopping scheme was redesigned to allow for a single chopper instead of two synchronized choppers.

#### TEA Lasers

Parts were ordered that were required to repair both TEA lasers and their power supplies. By interchanging parts, we were able to test-fire one of the TEA lasers. Since we observed intermittent arcs from the plasma chamber, we dismantled both lasers and cleaned/polished the nickel electrodes. The operable laser was then aligned and tested with the gain cell removed. Pulse energies of 80-90 mJ were obtained with multimode operation on 10P20. Significant power reduction (more than 50%) was observed with the gain cell inserted but not ignited. (The gain cell discharge tubes were tested separately.) We were ready to clean and realign the gain cells to check full up operation.



### Transmit/Receive Design Considerations

Relative performance evaluations were made of the MAPM system as designed (tri-static with small transmitter optics) to a possible coaxial system closer in transmit/receive geometry to the Doppler system. The major advantage to the latter was that it allows for sizable transmit and receive apertures (10"-12") with similar scanner clear apertures. Due to the tri-static nature of the existing design and despite the small transmit apertures (about 6"), large (24") scanner apertures would be required. This resulted in the large and cumbersome scanner mechanism which was basically incapable of elevation scans and which would almost certainly have led to azimuth dependent alignment problems due to astigmatism and other owing effects in the large flats. We did not think that the scanner system as designed would be capable of performing measurements without realignment at each azimuth. The major drawback to a coaxial DIAL system is that, since polarization states are already used to multiplex transmit and receive axes, there is no efficient means of combining the two transmit pulses without losses. We assumed in our performance evaluation that the beam combination is done with a 50-50 beamsplitter with resultant 50% losses in transmit energies. Despite this the conceptual coaxial system would still somewhat outperform the existing design at relevant ranges due to the larger transmit aperture and the better overlap.

We, in addition, had been evaluating the receive optics of the MAPM system. The roughly 12" f/5 parabolic receiver primary was somewhat of an enigma. Being only 5" off-axis it was impossible to use as planned without some obscuration. More importantly, there was in the existing design no true secondary element; without a collimating parabolic secondary there was no advantage to employing an expensive parabolic element in the first place. Indeed the introduction by the parabolic primary of unbalanced "spherical" aberrations probably reduced the system's heterodyne efficiency. We proceeded with evaluating whether desired performance could be achieved at reasonable cost with a spherical primary/secondary pair.

## **2.10 TENTH QUARTER**

### **2.10.1 CO<sub>2</sub> LIDAR SYSTEM**

#### "Real-Time" Ballistics Software

The data taken at UTTR consisted of four basic types: (1) lidar data and wind profiles from both the PL and NOAA systems; (2) ground impact locations; (3) cine-theodilte tracking of both the A/C nose and projectile; and (4) A/C release data. We reanalyzed all the PL lidar

data for final refined wind field data. The ambiguity in and frame of reference for ground impact locations were cleared up by using interpolated impact points from the cine-T data where overlap existed. After fitting for ground measurement origin and azimuthal axis rotation, the impact locations obtained from direct crater measurements and those obtained from interpolated trajectory data agreed surprisingly well--about 2-3 foot rms deviation. The final analysis was to compare the predicted down and cross range impact locations from the GPS A/C release data with the actual impacts as determined from the cine-T and ground impact data. The results showed rms cross range deviations of 100-200 feet for unmodified releases and about 20 feet for lidar wind profile modified releases.

#### CO<sub>2</sub> System Operation

We assisted with specification and ordering of replacement scanner mirrors for the Doppler lidar. We also began specifying the mechanical modifications required for mounting thicker scanner mirrors as well enabling reliable full 360 degree azimuth rotations. We also assisted in arranging for repair of the trailer suspension as well in reorganization of the trailer interior.

#### **2.10.2 MAPM**

Work continued in this quarter on the repair, refurbishment, and redesign of the MAPM DIAL system.

#### CW Lasers and LO Optics

A variable aperture chopper was obtained and modified to provide two out of phase trigger signals. Use of this chopper would obviate the need for the two synchronized choppers used in the original MAPM scheme.

#### TEA Lasers

Replacement high voltage components were obtained for the TEA laser modulators. We installed these circuits and tested both TEA laser discharge systems. In addition, the MPB EMT's and drivers were received and installed as replacements for the piezo-electric translators previously used for cavity length control. Both TEA lasers were now basically fully functioning. The components required for an AFC system were built or designed. Testing and installation of this frequency locking system was planned as the next major goal.

## **2.11 ELEVENTH QUARTER**

### **2.11.1 BALLISTIC WIND PROGRAM**

We completed analysis of the UTTR B52 data and assisted with its preparation for presentation. We also worked on evaluation of possible sites for future tests: Eglin AFB, UTTR, and WSMR. For these comparisons, we prepared histories at these sites of atmospheric transmission of 10.6 micron light from ground level to high altitude based on 1993 radiosonde data for the appropriate months. We also provided estimates of expected ballistic wind corrected misses versus release altitude for Mark 82 bombs under jet conditions. In addition, we assisted with modification of MBW--the code used for real time ballistic analysis--to enable direct reading of radiosonde data format as well as wind profile plotting. During this time period, we commenced writing a technical report on the GPOL Ballistic Wind Program to date--i.e., including the C130H gunship Eglin AFB as well as the B52 UTTR measurements. We also helped prepare the trailer for cold shipment to the next ballistic wind measurement site.

### **2.11.2 CO<sub>2</sub> DOPPLER LIDAR SYSTEM**

We assisted with: modifications of the trailer air ride; redesign of data acquisition and scanner computer interfaces; inspection and replacements of system optics; and modification of the trailer equipment layout. In addition, we: specified and ordered a lens to correct the laser beam profile to more accurately match that required by the telescope; built a mount for this lens; designed and built Brewster window covers with facility for clean N<sub>2</sub> flow--six of these were built for final installation on the MAPM as well as Doppler lasers; obtained replacement CO<sub>2</sub> TEA bellows for those broken on the return trip from UTTR. We also consulted on the Canetics i860 card software required for replacement of the existing DSP32c.

## **2.12 TWELFTH QUARTER**

### **2.12.1 BALLISTIC WIND PROGRAM**

We assisted with packing the Doppler lidar trailer for shipment to WSMR and specifying required field support. We also consulted on the required nature and accuracy of the aircraft track and bomb impact data. We worked on the operational fine points of the ballistics code--MBW. For mission planning and preparation, we prepared simulation studies of ballistic wind effects on high altitude unguided weapon releases as a function of wind speed,

profile, and direction relative to AC heading. For these simulations, we used synthetic profiles as well as meteorological and climatological data.

At WSMR (3/28-4/14), we worked on placement of the lidar trailer and set up the system. We also assisted in specifying required tactical and technical support. During the missions on 4/7 and 4/11, we acquired real time wind profiles and provided them for ballistics' analysis. We assisted in repacking the trailer for shipment back to Hanscom AFB.

The residual period of this quarter was spent on the initial analysis of the WSMR data. We wrote an algorithm for reduction of the raw data from the Oscuro Range toss cameras. The results were correlated with the DMA impact surveys to unambiguously assign aircraft releases with surveyed craters. For this preliminary analysis, we used the flight log data for AC track and position. The range theodolite data and data from the aircraft tapes did not arrive in time for inclusion into this first look analysis. This data would be used in the final analysis to be done early next quarter.

## **2.13 THIRTEENTH QUARTER**

### **2.13.1 BALLISTIC WIND PROGRAM**

We completed the final analysis of the WSMR data. Marked improvement in accuracy was found for modified releases in the jet stream over Oscuro Range on 4/11/94. Analysis of the ground impact and AC release data agreed well with the UTTR tests. For low wind cases, present release system timing bias and jitter as well as piloting error will dominate wind induced errors. We assisted in preparing this data for presentation. In addition, we ran a number of simulations based on meteorological and climatological data.

We consulted on the planned 2 micron airborne Doppler lidar--the next stage in the Ballistic Winds program. We were preparing a short report on the requirements for data acquisition and processing.

### **2.13.2 CO<sub>2</sub> DOPPLER LIDAR**

The TEA laser bellows were again damaged on the return trip from WSMR. We had these repaired using a more robust stainless steel stock and expected to test them early in the next quarter. In addition, we have consulted on the possibility of employing this system to test speckle reduction by mode locking the TEA laser. We expected to make and test the required modifications in the next quarter.

### **2.13.3 MAPM**

During this quarter, we:

- designed a preliminary optical layout for the revamped DIAL system;
- assisted in specifying/ordering the scanner and telescope;
- installed and tested one of the new cw MPB lasers;
- began redesigning the laser cooling water supply and interlocks;
- arranged a test installation for laser characterization;
- began work on TEA laser frequency stabilization.

We also assisted with MAPM trailer maintenance and layout.

## **2.14 FOURTEENTH QUARTER**

### **2.14.1 BALLISTIC WIND PROGRAM**

We consulted on the planned 2 micron airborne Doppler lidar--the next stage in the Ballistic Winds program. We assisted in making sensitivity and performance measurements on the LWE 2 micron lidar. We were preparing a report from these measurements on the expected performance of this system. We also worked on the software and hardware requirements for a data acquisition and processing system.

### **2.14.2 CO<sub>2</sub> DOPPLER LIDAR/FLD MODE LOCKING**

We extended the TEA CO<sub>2</sub> laser cavity to about 1.8 m to produce a cavity free spectral range (FSR) of about 80 MHz. We tested the AOM supplied by Textron to find the resonance closest to one half of the FSR. To reduce losses due to the small AOM aperture, we also had to alter the cavity mode geometry by using an intracavity lens. Initial mode locking measurements were made.

### **2.14.3 MAPM**

During this quarter, we constructed the electronics for TEA laser frequency stabilization using analog limiter/discriminator components. Our initial tests showed some locking instabilities which may have been related to the gain cell seeding of these lasers. We begun to assemble the components for a data acquisition system similar to that used in the Doppler system. This would allow real time characterization of the frequency chirp and spread.

## **2.15 FIFTEENTH QUARTER**

### **2.15.1 BALLISTIC WIND PROGRAM**

We consulted on the planned 2 micron airborne Doppler lidar. Measurements and simulations indicated that the LWE transceiver was inadequate in its existing form for high altitude remote wind sensing. We also made engineering and sensitivity studies of other possible transmitters which concluded that the performance required for the mission and the engineering required for unmanned operation in an uncontrolled environment could not be met without a 1-3 year development program. The bomber Ballistic Wind program was redirected towards a next step concept demonstration involving the Wright labs C-141 based lidar. Towards this end, we assisted in evaluating this system and outlining the concept of operations for the demonstration flight.

### **2.15.2 CO<sub>2</sub> DOPPLER LIDAR/FLD MODE LOCKING**

The two mode target speckle reduction measurements were made and analyzed. They confirmed the reduction in the intermodal speckle correlation at near grazing angles. The results of these tests were communicated to interested parties. In addition, we constructed a fast RF switch in order to gate the nominal 40 MHz drive to the AOM used to frequency shift the seed. This would improve the low SNR performance of the Doppler system by eliminating optical and electronic contamination of the signal. It would also allow us to shift upward the seed frequency by several MHz in order to compensate for chirp.

### **2.15.3 MAPM**

We continued optical and electronic design and specification for MAPM system components, including a complex demodulator, data acquisition/processing, laser stabilization, and transmit/receive optics. Initial reconditioning of the MAPM TEA lasers showed that one of the HV power supplies was malfunctioning. We had been using the spare HV supply from the Doppler system. Failure of the HV power supply to the Doppler TEA laser this quarter required that we take this spare back. This raised repair of these supplies to a higher priority. We began assembling documentation for these units prior to repairing them. We also began discussions with DFM, Inc. on scanner design, costs, and integration.

## **2.16 SIXTEENTH QUARTER**

### **2.16.1 BALLISTIC WIND PROGRAM**

The bomber Ballistic Wind program had been redirected towards a next step concept demonstration involving the Wright Labs C-141 based lidar. Towards this end, we consulted with GPOL and WL personnel on the performance of the WL system as well as on required software/hardware/operating system modifications to calculate ballistic wind corrections in near real time from the WL lidar data. Two techniques were considered: (1) incorporating the algorithms we used on previous BW demonstrations into the WL lidar data acquisition system, and/or (2) using a separate laptop computer on the C-141. In the latter case, hardware and drivers would be required to transfer data from the workstation/UNIX platform to a laptop PC/DOS platform.

### **2.16.2 CO<sub>2</sub> DOPPLER LIDAR/FLD SPECKLE MEASUREMENTS**

We began a technical report on the two mode target speckle reduction measurements made in the last quarter.

The AOM switching circuit constructed in the last quarter was fully tested and would be used on the planned July BW demonstration. In addition, we worked on modifications to the scanner to allow for reliable full 360 degree scans without flipping the elevation mirror. We also fully tested use of a correction lens to better collimate the TEA laser output beam.

## **2.17 SEVENTEENTH QUARTER**

### **2.17.1 BALLISTIC WIND PROGRAM**

A new version of the MBW (3.1) code was completed for use on the June tests at UTTR. This version incorporated software for data transfer from a UNIX tar format tape drive--the media used by the WL PADDL system. Other data file transfer and editing features were included to allow the operator flying with the WL C141 options for manipulating the wind profiles.

Additions were also made to the Doppler lidar operating system (IQV5). A scanning graphics bar was included to inform the operator of the remaining time in a scan. The laser PSD was now plotted in real time on data acquisition runs so that the operator could monitor the laser and locking system performance. To obtain the time for the above processes, we changed the procedure for data transfer to the DSP cards--we replaced the DMA process previously used with assembler string copy routines. This saved several milliseconds of host time which was sufficient for maintenance of the scan bar and laser spectral profile plotting.

We assisted with the packing, shipping, setup, and operation of the Doppler lidar for the WPAFB and UTTR field tests. During the UTTR field tests, we also operated the MBW code to obtain real time wind corrections using ground lidar and radiosonde data. After the UTTR tests, we prepared preliminary reports on the wind and impact data.

### **2.17.2 CO<sub>2</sub> DOPPLER LIDAR/FLD SPECKLE MEASUREMENTS**

We did no further work on the technical report on the two mode target speckle reduction measurements.

### **2.17.3 MAPM**

We continued optical and electronic design and specification for MAPM system components, including a complex demodulator, data acquisition/processing, laser stabilization, and transmit/receive optics.

TEA lasers were moved back to the lower deck. Dust covers were made and installed for the CW and TEA lasers. Cooling water for all four lasers was rerouted to a gang valve panel using a single water chiller (for simplification.)

Propagation of a less divergent CW laser beam (by using a +40 cm focal length lens directly in front of the laser) was studied and measured in order to ensure that the backward propagated CW and outgoing TEA pulse could be matched both in size and field curvature.

Optics for the redesign were specified and sources for these optics were identified. These optical elements included: converging lenses for the CW lasers, non-diverging output couplers for the TEA lasers, beam splitters, Fresnel Rhomb, and CW beam expander. Price quotes and specifications were obtained from several vendors.

Layout of all optical components was completed following the draft specification of the telescope geometry. A compilation of pollutant absorption coefficients at the CO<sub>2</sub> laser lines was started. Of specific interest was the interference that ambient atmospheric species would have on the DIAL results.

## **2.18 EIGHTEENTH QUARTER**

### **2.18.1 BALLISTIC WIND PROGRAM**

We statistically analyzed the UTTR 95 impact data from both the real time triangulation and post-mission surveys. Included in this treatment was a breakdown by release type and comparison to expected wind induced errors. Because the cine-theodolite data was incomplete, we had not been able to do a complete analysis in which platform and release



errors were extracted. We prepared a preliminary final report on the PL/GPOL high altitude ballistic wind program.

We also obtained a copy of the raw airborne 2 micron lidar data taken by WL at UTTR. We transcribed this data from tape to hard disk, deciphered its format, and wrote software for its analysis. We assisted with preparation of a briefing for General Paul based on this analysis and the results of the UTTR 93, WSMR 94, and UTTR 95 missions.

### **2.18.2 MAPM**

Optics for the redesigned system were ordered. These optical elements included: converging lenses for the CW lasers, non-diverging output couplers for the TEA lasers, beam splitters, Fresnel Rhomb, and CW beam expander. Also ordered, were an XYZ-mount for the beam expander and a tiltable+focus mount for the signal lens in front of the HgCdTe detector.

Consultations about the scanner mount were continued. We settled on a table mount design for the scanner (instead of a floor mount) after considering the locations and footprints on the optics table for the telescope and kick mirror. The definition of the modifications required for the trailer the design of the mounting structure for the scanner were completed.

The trailer was packed up for the scanner modifications. All optics and mounts were removed from the table. The TEA lasers were left in place on the lower table after being covered and tied down. The trailer went to the GP machine shop at the end of this quarter for modifications required for the scanner installation. The GP machine shop would be building the mounting structure and installing the scanner to be sure the mechanical design was correct.

Operating wavelengths ranges of the CW lasers were measured. A compilation of pollutant absorption coefficients at these accessible CO<sub>2</sub> laser lines was complete. It appeared that interference from ambient atmospheric species would have an effect on the DIAL results for the measurement of certain pollutants.

### **2.18.3 SBIRS CIRRUS DATA**

We ran the PL/GPOL CO<sub>2</sub> lidar in support of a SBIRS data overflight of Hanscom AFB. The lidar was, for the most part, operated in a vertical backscatter mode with 100-1000 pulse averages continuously taken for 5 hours. We transformed this data into a cirrus 2-d time/altitude gray scale image which was provided to PL/GPOL and interested SBIRS parties.

## **2.19 NINETEENTH QUARTER**

### **2.19.1 MAPM**

The demodulation electronics were built and bench tested during this period. Included within the large demodulation 'box' was a card to generate the automatic frequency control gate with variable delay and width. This gate outputs a signal to a fast GaAs switch which channels the AFC signal to the digitizer (in lieu of the return signal) during a short user selected laser firing interval. Also in the box are the electronics (such as the 40 MHz Limiter/Discriminator) required for conditioning the AFC signal for the boxcar samplers.

The trailer was returned to upper parking space #2 with the scanner installed. To be moved out of the high bay, the large bay door was manually opened above the top flange of the door frame and air was let out of the trailer's tires which lowered the back end of the trailer by about two inches.

The optics table was cleared for the expected installation of the telescope.

### **2.19.2 BALLISTIC WIND PROGRAM**

During this period we continued work on a final report on the B52 ballistic winds program. In addition, we began preparation of a paper on this program for presentation at the May, 1996 Active IRIS conference. We also consulted with GPOL and Wright Laboratory personnel on providing ground truth lidar winds at Yuma Proving Grounds in February 1996 for an Airdrop Ballistic Winds trial. We also wrote and provided to the 49 TEST Squadron a modified version of the MBW code used to determine ballistic wind correction vectors.

### **2.19.3 SBIRS CIRRUS DATA**

We carried out further analysis of the cirrus cloud data taken in support of a SBIRS data overflight of Hanscom AFB. This analysis included algorithms to determine cloud bottom and top versus time as well as to provide cloud density plots in several different formats.

## **2.20 TWENTIETH QUARTER**

### **2.20.1 MAPM**

The telescope was installed on 2 February 1996. Once in place and bolted to the table, the rest of the optics could be put back into position. The first of the plexiglass dust covers was installed over the CW lasers. Removal of the interior wall (by the shop) allowed for the rearrangement of some of the equipment racks and cabinets into more user friendly positions.

A custom base was made for the local oscillator chopper wheel. Also, a mounting ring was fabricated to hold the 2x beam expander in its 5-axis mount. The thin film polarizer (TFP) and Rhomb were mounted on posts just in front of the telescope. We installed a kinematic mount on the last mirror before the AFC detector so that we would have the capability to quickly confirm the line(s) on which the laser(s) are operating. A change of alignment procedure was required because the new TFP was not transparent in the visible so that the optical path of the HeNe (coaligned with the pulsed lasers) could not be followed into the telescope. Instead, a HeNe on the upper table is backward propagated by back reflections from the LO beam expander. A 2-inch diameter 50/50 beam splitter is now in place on the lower deck so now the two TEA lasers can be combined.

The scanner checkout did not go well. The control electronics had been poorly packaged for shipment by the manufacturer which resulted in connectors and wires being pulled out of a computer interface board. The initial attempts at simple manual operation of the scanner sent it into a runaway mode. Cables were mislabeled (and thus crossed) and an encoder was malfunctioning. Cables were uncrossed and a new encoder was installed. The scanner was then functional.

#### **2.20.2 BALLISTIC WIND PROGRAM**

During this period we continued work on a final report on the B52 ballistic winds program. In addition, we completed preparation and submission of a paper on this program for presentation at the May, 1996 IRIS Active System conference at Eglin AFB, FL.

We also carried out field Doppler lidar tests at Yuma Proving Grounds. During this program, we provided real-time wind profiles to Wright Laboratory personnel. In addition, we provided them with post-mission analysis of aerosol signal levels versus altitude.